Future snowfall in the Alps: Projections based on the EURO-CORDEX regional climate models

Prisco Frei, Sven Kotlarski, Mark A. Liniger, Christoph Schär

- Third response to referees and to editor -

We thank both the anonymous reviewer and the editor for another thorough check of the revised manuscript and for taking the effort to replicate one of our reply figures. We are sorry that we could not appropriately address one remaining concern regarding the final selection of climate models. The reviewer is completely right, Figure R1 in our replies showed the summer season JJA only. We are sorry for this mistake and for not specifying the underlying time period properly in the figure caption.

Indeed, the snow (accumulation) issue in terms of an obvious feedback to the temperature change signal is most pronounced in summer. But as we already mentioned before, deficiencies especially of the two RACMO model chains (EC-EARTH-RACMO and HadGEM2-RACMO) in adjacent seasons cannot be excluded. As we show in the new Figures S11 and S12 of the revised manuscript, these deficiencies indeed remain at least for the two adjacent months May and September which are considered in our analysis. And it is only these two model chains that are obviously affected. IPSL-WRF does not seem to be problematic, but this model chain has further obvious deficiencies that in our opinion justify a removal from at least parts of the analysis. Please note that the IPSL-WRF issue became apparent in the context of the CH2018 model selection and after(!) submission of the initial manuscript. We believe that, with this additional information, it is valid to modify the set of models considered during the revision phase of a paper if properly motivated. EC-EARTH-RACMO has been removed from the analysis following a hint of the reviewer himself, for which we are thankful.

To accommodate the remaining concerns of the reviewer and the suggestions of the editor we now revised our manuscript and implemented several changes. These changes imply a consideration of potentially deficient model simulations in the analysis, but only in places where the identification of individual experiments is possible. In these cases we now consider the original ensemble of 14 GCM-RCM chains for each emission scenario (*full set*). This set comprises EC-EARTH-RACMO and IPSL-WRF. For ensemble-based analyses that do only present multi-model mean and ranges, we however employ a reduced set of 12 model chains only (*reduced set*). The composition of the two sets is described in Table 1. The motivation for removing individual simulations from the available set of all simulations is summarized in Chapter 2.2 and fully motivated (including several additional figures) in the new Supplementary Material, Part B. An additional Figure S15 is included that corresponds to the central result Figure 12 of the main manuscript but employs the full instead of the reduced model set. A comparison of both figures indicates only minor influences of the model selection on the main results and conclusions and, hence, a robust ensemble analysis that does not strongly depend on shortcomings of individual simulations. This fact is now prominently mentioned in the conclusions of the manuscript.

In addition to this, we corrected several typos and slightly modified the phrasing at a few places throughout the manuscript.

We hope that the revised version of the paper accommodates the remaining concerns and is considered as being appropriate. Please find the new version with all changes highlighted in the attachment. We are looking forward to your decision.

With kind regards,

Sven Kotlarski
(on behalf of all co-authors)

New manuscript version with marked-up changes:

Future snowfall in the Alps: Projections based on the EURO-CORDEX regional climate models

Prisco Frei [1], Sven Kotlarski [2,*], Mark A. Liniger [2], Christoph Schär [1]

[1] Institute for Atmospheric and Climate Sciences, ETH Zurich, CH-8006 Zurich, Switzerland
[2] Federal Office of Meteorology and Climatology, MeteoSwiss, CH-8058 Zurich-Airport, Switzerland

[*] Corresponding author: *sven.kotlarski@meteoswiss.ch*

Abstract. Twenty-first century snowfall changes over the European Alps are assessed based on high-resolution regional climate model (RCM) data made available through the EURO-CORDEX initiative. Fourteen different combinations of global and regional climate models with a target resolution of 12 km, and two different emission scenarios are considered. As raw snowfall amounts are not provided by all RCMs, a newly developed method to separate snowfall from total precipitation based on near-surface temperature conditions and accounting for subgrid-scale topographic variability is employed. The evaluation of the simulated snowfall amounts against an observation-based reference indicates the ability of RCMs to capture the main characteristics of the snowfall seasonal cycle and its elevation dependency, but also reveals considerable positive biases especially at high elevations. These biases can partly be removed by the application of a dedicated RCM bias adjustment that separately considers temperature and precipitation biases.

Snowfall projections reveal a robust signal of decreasing snowfall amounts over most parts of the Alps for both emission scenarios. Domain and multi-model mean decreases of mean September-May snowfall by the end of the century amount to -25% and -45% for RCP4.5 and RCP8.5, respectively. Snowfall in low-lying areas in the Alpine forelands could be reduced by more than -80%. These decreases are driven by the projected warming and are strongly connected to an important decrease of snowfall frequency and snowfall fraction and are also apparent for heavy snowfall events. In contrast, high-elevation regions could experience slight snowfall increases in mid-winter for both emission scenarios despite the general decrease of the snowfall fraction. These increases in mean and heavy snowfall can be explained by a general increase of winter precipitation and by the fact that, with increasing temperatures, climatologically cold areas are shifted into a temperature interval which favours higher snowfall intensities. In general, percentage changes of snowfall indices are robust with respect to the RCM postprocessing strategy employed: Similar results are obtained for raw, separated and separated + bias-adjusted snowfall amounts. Absolute changes, however, can differ among these three methods.

1 Introduction

Snow is an important resource for the Alpine regions, be it for tourism, hydropower generation, or water management (Abegg et al., 2007). According to the Swiss Federal Office of Energy (SFOE) hydropower generation accounts for approximately 55% of the Swiss electricity production (SFOE, 2014). Consideration of changes in snow climatology needs to address aspects of both snow cover and snowfall. In the recent past, an important decrease of the mean snow cover depth and duration in the Alps was observed (e.g, Laternser and Schneebeli, 2003; Marty, 2008; Scherrer et al., 2004). Projections of future snow cover changes based on climate model simulations indicate a further substantial reduction (Schmucki et al., 2015a; Steger et al., 2013), strongly linked to the expected rise of temperatures (e.g., CH2011, 2011; Gobiet et al., 2014). On regional and local scales rising temperatures exert a direct influence on snow cover in two ways: First, total snowfall sums are expected to decrease ~~by~~ as a result of a lower probability for precipitation to fall as snow, implying a decreasing overall snowfall fraction (ratio between solid and total precipitation). Second, snow on the ground is subject to faster and accelerated melt. These warming-induced trends might be modulated, for instance, by changes in atmospheric circulation patterns.

Although the snowfall fraction is expected to decrease during the 21st century (e.g., Räisänen, 2016) extraordinary snowfall events can still leave a trail of destruction. A recent example was the winter 2013/2014 with record-breaking heavy snowfall events along the southern rim of the European Alps (e.g., Techel et al., 2015). The catastrophic effects of heavy snowfall range from avalanches and floods to road or rail damage. In extreme cases these events can even result in the weight-driven collapse of buildings or loss of human life (Marty and Blanchet, 2011). Also mean snowfall conditions, such as the mean number of snowfall days in a given period, can be of high relevance for road management (e.g. Zubler et al., 2015) or airport operation. Projections of future changes in snowfall, including mean and extreme conditions, are therefore highly relevant for long-term planning and adaptation purposes in order to assess and prevent related socio-economic impacts and costs.

21st century climate projections typically rely on comprehensive climate models. For large-scale projections, global climate models (GCMs) with a rather coarse spatial resolution of 100 km or more are used. To assess regional to local scale impacts, where typically a much higher spatial resolution is required, a GCM can be dynamically downscaled by nesting a regional climate model (RCM) over the specific domain of interest (Giorgi, 1990). In such a setup, the GCM provides the lateral and sea surface boundary conditions to the RCM. One advantage of climate models is their ability to estimate climate change in a physically based manner under different greenhouse gas (GHG) emission scenarios. With the Intergovernmental Panel on Climate Change's (IPCC) release of the Fifth Assessment Report (AR5; IPCC, 2013) the so-called representative concentration pathway (RCP) scenarios have been introduced (Moss et al., 2010) ~~which~~. These specify GHG concentrations and corresponding emission pathways for several radiative forcing targets. To estimate inherent projection uncertainties, ensemble approaches employing different climate models, different greenhouse gas scenarios, and/or different initial conditions are being used (e.g., Deser et al., 2012; Hawkins and Sutton, 2009; Rummukainen, 2010).

Within the last few years several studies targeting the future global and European snowfall evolution based on climate model ensembles were carried out (e.g., de Vries et al., 2013; de Vries et al., 2014; Krasting et al., 2013; O'Gorman, 2014; Piazza et al., 2014; Räisänen, 2016; Soncini and Bocchiola, 2011). Most of these analyses are based on GCM output or older generations of RCM ensembles at comparatively low spatial resolution, which are not able to properly resolve snowfall events over regions with complex topography. New generations of high resolution RCMs are a first step toward an improvement on this issue. This is in particular true for the most recent high-resolution regional climate change scenarios produced by the global CORDEX initiative (Giorgi et al., 2009) and its European branch EURO-CORDEX (Jacob et al., 2014). The present work aims to exploit this recently established mutli-model archive with respect to future snowfall conditions over the area of the European Alps. It thereby complements the existing works of Piazza et al. (2014) and de Vries et al. (2014). These two works also exploit comparatively high-resolved RCM experiments but with a smaller focus domain in the case of Piazza et al. (2014; French Alps only) and based on a single-model ensemble with a comparatively small ensemble size (eight members) in the case of de Vries et al. (2014).

In general and on decadal to centennial time scales, two main drivers of future snowfall changes over the European Alps with competing effects on snowfall amounts are apparent from the available literature: (1) Mean winter precipitation is expected to increase over most parts of the European Alps and in most EURO-CORDEX experiments (e.g., Rajczak et al., 2017; Smiatek et al., 2016) which in principle could lead to higher snowfall amounts. (2) Temperatures are projected to considerably rise throughout the year (e.g., Gobiet et al., 2014; Smiatek et al., 2016; Steger et al., 2013) with the general effect of a decreasing snowfall frequency and fraction, thus potentially leading to a reduction in overall snowfall amounts. Separating the above two competing factors is one of the targets of the current study. A potential complication is that changes in daily precipitation frequency (events with precipitation > 1 mm/day) and precipitation intensity (average amount on wet days) can change in a counteracting manner (e.g., Fischer et al., 2015; Rajczak et al., 2013), and that relative changes are not uniform across the event category (e.g.; Fischer and Knutti, 2016; Rajczak et al., 2017).

We here try to shed more light on these issues by addressing the following main objectives:

Snowfall separation on the RCM grid. Raw snowfall outputs are not available for all members of the EURO-CORDEX RCM ensemble. Therefore, an adequate snowfall separation technique, i.e., the derivation of snowfall amounts based on readily available daily near-surface air temperature and precipitation data, is required. Furthermore, we seek for a snowfall separation method that accounts for the topographic subgrid-scale variability of snowfall on the RCM grid.

Snowfall bias adjustment. Even the latest generation of RCMs is known to suffer from systematic model biases (e.g., Kotlarski et al., 2014). In GCM-driven setups as employed within the present work these might partly be inherited from the driving GCM. To remove such systematic ~~model~~ biases in temperature and precipitation, a dedicated ~~simple~~ bias adjustment method is developed and employed in the present work. To assess its performance and applicability, different snowfall indices in the bias-adjusted and not bias-adjusted output are compared against observation-based estimates.

Snowfall projections for the late 21st century. Climate change signals for various snowfall indices over the Alpine domain and for specific elevation intervals, derived by a comparison of 30-year control and scenario periods, are analysed under the assumption of the RCP8.5 emission scenario. In addition, we aim to identify and quantify the main drivers of future snowfall changes and, in order to assess emission scenario uncertainties, compare RCP8.5-based results with experiments assuming the more moderate RCP4.5 emission scenario. Snowfall projections are generally based on three different datasets: (1) raw RCM snowfall where available, (2) RCM snowfall separated from simulated temperature and precipitation, and (3) RCM snowfall separated from simulated temperature and precipitation and additionally bias-adjusted. While all three estimates are compared for the basic snowfall indices in order to assess the robustness of the projections, more detailed analyses are based on dataset (3) only.

In addition and as preparatory analysis, we carry out a basic evaluation of RCM-simulated snowfall amounts. This evaluation, however, is subject to considerable uncertainties as a high-quality observation-based reference at the required spatial scale is not available, and the focus of the present work is laid on snowfall projections.

The article is structured as follows: Section 2 describes the data used and methods employed. In Sections 3 and 4 results of the bias adjustment approach and snowfall projections for the late 21st century are shown, respectively. The latter are further discussed in Section 5 while overall conclusions and a brief outlook are provided in Section 6. Additional supporting figures are provided in the S~~s~~upplementary M~~m~~aterial (prefix 'S' in f~~F~~igure numbers).

2 Data and methods

2.1 Observational data

To estimate the reference fine-scale snowfall, two gridded data sets, one for precipitation and one for temperature, derived from station observations and covering the area of Switzerland are used. Both data sets are available on a daily basis with a horizontal resolution of 2 km for the entire evaluation period 1971-2005 (see Sec. 2.3).

The gridded precipitation data set (RhiresD) represents a daily analysis based on a high-resolution rain-gauge network (MeteoSwiss, 2013a) consisting of more than 400 stations that have a balanced distribution in the horizontal but under-represent high altitudes (Frei and Schär, 1998; Isotta et al., 2014; Konzelmann et al., 2007). Albeit the data set's resolution of 2 km, the effective grid resolution as represented by the mean inter-station distance is about 15 - 20 km and thus comparable to the nominal resolution of the available climate model data (see Sec. 2.2). The dataset has not been corrected for the systematic measurement bias of rain gauges (e.g., Neff, 1977; Sevruk, 1985; Yang et al., 1999).

The gridded near-surface air temperature (from now on simply referred to as *temperature*) data set (TabsD) utilises a set of approx. 90 homogeneous long-term station series (MeteoSwiss, 2013b). Despite the high quality of the underlying station series, errors might be introduced by unresolved scales, an uneven spatial distribution and interpolation uncertainty (Frei, 2014). The unresolved effects of land cover or local topography, for instance, probably lead to an underestimation of spatial variability. Also note that, while RhiresD provides daily precipitation sums aggregated from 6 UTC to 6 UTC of the following day, TabsD is a true daily temperature average from midnight UTC to midnight UTC. Due to a high temporal autocorrelation of daily mean temperature this slight inconsistency in the reference interval of the daily temperature and precipitation grids is expected to not systematically influence our analysis.

In addition to the gridded temperature and precipitation datasets and in order to validate simulated raw snowfall amounts station-based observations of fresh snow sums (snow depth) at daily resolution from 29 stations in Switzerland with data available for at least 80% of the evaluation period 1971-2005 are employed.

2.2 Climate model data

In terms of climate model data we exploit a recent ensemble of regional climate projections made available by EURO-CORDEX (www.euro-cordex.net), the European branch of the World Climate Research Programme's CORDEX initiative (www.cordex.org; Giorgi et al., 2009). RCM simulations for the European domain were run at a resolution of approximately 50 km (EUR-44) and 12 km (EUR-11) with both re-analysis boundary forcing (Kotlarski et al., 2014; Vautard et al., 2013) and GCM ~~-~~forcing (Jacob et al., 2014). We here disregard the reanalysis-driven experiments and employ the GCM-driven simulations only. These include historical control simulations and future projections based on RCP greenhouse gas and aerosol emission scenarios. ~~Within the present work w~~We employ daily averaged model output of GCM-driven EUR-11 simulations that were available in December 2016 and for which control, RCP4.5 and RCP8.5 runs are ~~available~~provided. ~~Individual available experiments were disregarded due to serious simulation shortcomings that potentially affect our analysis [1]. . The exclusion of these experiments is in line with the current set of experiments considered for the upcoming CH2018 Swiss climate scenarios (www.ch2018.ch). In total, a set of 12 GCM-RCM model chains is considered, combining five driving GCMs with five different RCMs (Tab. 1).~~ We hence exclusively focus on the higher resolved EUR-11 simulations and disregard the coarser EUR-44 ensemble due to the apparent added value of the EUR-11 ensemble with respect to regional-scale climate features in the complex topographic setting of the European Alps (e.g., Giorgi et al., 2016; Torma et al., 2015). Out of the entire set of available EURO-CORDEX simulations, several GCM-RCM chains were either completely or partially removed from our analysis, resulting in a full set of 14 GCM-RCM combinations and a reduced set of 12 combinations only (Table 1). Reasons for removal are the existence of several realisations (MPI-ESM-REMO; only one realisation has been used) and serious simulation deficiencies that potentially affect our analysis (HadGEM2-RACMO, EC-EARTH-RACMO and IPSL-WRF). Further details on these issues are provided in the Supplementary Material, Part B.

~~[1] All experiments of the RACMO RCM were excluded due to serious snow accumulation issues and evident feedbacks on 2m temperatures over the European Alps. Also, the IPSL-driven WRF simulations were disregarded due to suspicious and probably unphysical climate change signals in summer over the Alpine domain. Furthermore, only realization 1 of MPI-M-REMO was included in order to avoid mixing GCM-RCM sampling with pure internal climate variability sampling.~~

It is important to note that each of the ~~five~~ RCMs considered uses an individual ~~grid cell~~ topography field. Model topographies for a given grid cell might therefore considerably differ from each other, and also from the observation-based orography. ~~Hence, i~~It is therefore not meaningful to compare snowfall values at individual grid cells since the latter might be situated at different elevations. ~~Therefore,~~For this reason most analyses of the present work were carried out as a function of elevation, i.e., by averaging ~~climatic features~~ quantities over distinct elevation intervals.

2.3 Analysis domain and periods

The arc-shaped European Alps - with a West-East extent of roughly 1200 km , a total of area 190'000 km^2 and a peak elevation of 4810 m a.s.l. (Mont Blanc) - are the highest and most prominent mountain range which is entirely situated in Europe. In the present work, two different analysis domains are used. The evaluation of the bias adjustment approach depends on the observational data sets RhiresD and TabsD (see Sec. 2.1). As these cover Switzerland only, the evaluation part of the study (Sec. 3) is constrained to the Swiss domain (Fig. 1, bold line). For the analysis of projected changes of different snowfall indices (Sec. 4 and 5) a larger domain covering the entire Alpine crest with its forelands is considered (Fig. 1, coloured region).

Our analysis is based on three different time intervals. The evaluation period (EVAL) 1971-2005 is used for the calibration and validation of the bias adjustment approach. Future changes of snowfall indices are~~-~~ computed by comparing a present-day control period (1981-2010, CTRL) to a future scenario period at the end of the 21st century (2070-2099, SCEN). For all periods (EVAL, CTRL and SCEN), the summer months June, July and August (JJA) are excluded from ~~any statistical~~ the analysis. In addition to seasonal mean snowfall conditions, i.e., averages over the nine-month period from September to May, we also analyse the seasonal cycle of individual snowfall indices at monthly resolution.

2.4 Analysed snowfall indices and change signals

A set of six different snowfall indices is considered (Tab. 2). Mean snowfall (S_{mean}) refers to the (spatio-)~~-~~temporally-averaged snowfall amount in mm SWE (note that from this point on we will use the term "mm" as a synonym for "mm SWE" as unit of several snowfall indices). The two indices heavy snowfall (S_{q99}) and maximum 1-day snowfall (S_{1d}) allow the assessment of projected changes in heavy snowfall events and amounts. S_{1d} is derived by averaging maximum 1-day snowfall amounts over all individual months/seasons of a given time period (i.e., by averaging 30 maximum values in the case of the CTRL and SCEN period), while S_{q99} is calculated from the grid point-based 99th all-day snowfall percentile of the daily probability density function (PDF) for the entire time period considered. We use all-day percentiles as the use of wet-day percentiles leads to conditional statements that are often misleading (see the analysis in Schär et al. 2016). Note that the underlying number of days differs for seasonal (September-May) and monthly analyses. Snowfall frequency (S_{freq}) and mean snowfall intensity (S_{int}) are based on a wet-day threshold of 1 mm/day and provide additional information about the distribution and magnitude of snowfall events, while the snowfall fraction (S_{frac}) describes the ratio of solid precipitation to total precipitation. As climate models tend to suffer from too high occurrence of drizzle and as small precipitation amounts are difficult to measure, daily precipitation values smaller or equal to 0.1 mm were set to zero in both the observations and the simulations prior to the remaining analyses.

Projections are assessed by calculating two different types of changes between the CTRL and the SCEN period. The absolute change signal (∆) of a particular snowfall index X (see Tab.2)

$$\Delta \boldsymbol{X} = \boldsymbol{X}_{SCEN} - \boldsymbol{X}_{CTRL} \quad (1)$$

and the relative change signal (δ) which describes the change of the snowfall index as a percentage of its CTRL period value

$$\boldsymbol{\delta X} = \left(\frac{X_{SCEN}}{X_{CTRL}} - \boldsymbol{1}\right) \cdot \boldsymbol{100} \quad (2)$$

To prevent erroneous data interpretation due to possibly large relative changes of small CTRL values, certain grid boxes were masked out before calculating and averaging the signal of change. This filtering was done by setting threshold values for individual indices and statistics (Tab. 2).

2.5 Separating snowfall from total precipitation

Due to (a) the lack of a gridded observational snowfall data set and (b) the fact that not all EURO-CORDEX RCMs provide raw snowfall as an output variable, a method to separate solid from total precipitation depending on near-surface temperature conditions is developed. The simplest approach to separate snowfall from total precipitation is to fractionate the two phases binary by applying a constant snow fractionation temperature (e.g., de Vries et al., 2014; Schmucki et al., 2015a; Zubler et al., 2014). More sophisticated methods estimate the snow fraction f_s dependence on air temperature with linear or logistic relations (e.g., Kienzle, 2008; McAfee et al., 2014). In our case, the different horizontal resolutions of the observational (high resolution of 2 km) and simulated (coarser resolution of 12 km) data sets further complicate a proper comparison of the respective snowfall amounts. Thus, we explicitly analysed the snowfall amount dependency on the grid resolution and exploited possibilities for including subgrid-scale variability in snowfall separation. This approach is important as especially in Alpine terrain a strong subgrid-scale variability of near-surface temperatures due to orographic variability has to be expected, with corresponding effects on the subgrid-scale snowfall fraction.

For this preparatory analysis, which is entirely based on observational data, a reference snowfall is derived. It is based on the approximation of snowfall by application of a fixed temperature threshold to daily total precipitation amounts on the high resolution observational grid (2 km) and will be termed *Subgrid method* thereafter: First, the daily snowfall S' at each grid point of the observational data set at high resolution (2 km) is derived by applying a snow fractionation temperature T^*=2°C. The whole daily precipitation amount P' is accounted for as snow S' (i.e., f_s=100%) for days with daily mean temperature $T' \leq T^*$. For days with $T' > T^*$, S' is set to zero and P' is attributed as rain (i.e., f_s=0%). This threshold approach with a fractionation temperature of 2°C corresponds to the one applied in previous works and results appear to be in good agreement with station-based snowfall measurements (e.g., Zubler et al., 2014). The coarse grid (12 km) reference snowfall S_{SG} is determined by averaging the sum of separated daily high resolution *S'* over all *n* high-resolution grid points *i* located within a specific coarse grid point *k*. I.e., at each coarse grid point *k*

$$S_{SG} = \frac{1}{n} \cdot \sum_{i=1}^{n} P'_i \, [T'_i \leq T^*] = \frac{1}{n} \sum_{i=1}^{n} S'_i \tag{3}$$

For comparison, the same binary fractionation method with a temperature threshold of T^*=2°C is directly applied on the coarse 12 km grid (*Binary method*). For this purpose, total precipitation *P'* and daily mean temperature *T'* of the high-resolution data are conservatively remapped to the coarse grid leading to *P* and *T*, respectively. Compared to the *Subgrid method*, the *Binary method* neglects any subgrid-scale variability of the snowfall fraction. As a result, the *Binary method* underestimates S_{mean} and overestimates S_{q99} for most elevation intervals (Fig. 2). The underestimation of S_{mean} can be explained by the fact that even for a coarse grid temperature above T^* individual high-elevation subgrid cells (at which $T' \leq T^*$) can receive substantial snowfall amounts. As positive precipitation-elevation gradients can be assumed for most parts of the domain (larger total precipitation at high elevations; see e.g. Kotlarski et al., 2012 and Kotlarski et al., 2015 for an Alpine-scale assessment) the neglect of subgrid-scale snowfall variation in the *Binary method* hence leads to a systematic underestimation of mean snowfall compared to the *Subgrid method*. Furthermore, following O'Gorman (2014), heavy snowfall events are expected to occur in a narrow temperature range below the rain-snow transition. As the *Binary method* in these temperature ranges always leads to a snowfall fraction of 100%, too large S_{q99} values would result.

To take into account these subgrid-scale effects, a more sophisticated approach – referred to as the *Richards method* – is developed here. This method is based upon a generalised logistic regression (Richards, 1959). Here, we apply this regression to relate the surface temperature *T* to the snow fraction f_s by accounting for the topographic subgrid-scale variability. At each coarse grid-point *k*, the *Richards method*-based snowfall fraction $f_{s,RI}$ for a given day is hence computed as follows:

$$f_{s,RI}(T_k) = \frac{1}{\left[1 + C_k \cdot e^{D_k \cdot (T_k - T^*)}\right]^{\frac{1}{C_k}}} \tag{4}$$

with *C* as the point of inflexion (denoting the point with largest slope), and *D* the growth rate (reflecting the mean slope). T_k is the daily mean temperature of the corresponding coarse grid box *k* and T^*=2°C the snow fractionation temperature. First, we estimate the two parameters *C* and *D* of Equation 4 for each single coarse grid point *k* by minimizing the least-square distance to the f_s values derived by the *Subgrid method* via the reference snowfall S_{SG} (local fit). Second, C and D are expressed as a function of the topographic standard deviation σ_h of the corresponding coarse resolution grid point only (Fig. S1; global fit). This makes it possible to define empirical functions for both *C* and *D* that can be used for all grid points *k* in the Alpine domain and that depend on σ_h only.

$$\sigma_{h,k} = \sqrt{\frac{\sum_i^n \left(h_i - \overline{h_k}\right)^2}{n-1}} \tag{5}$$

$$C_k = \frac{1}{(E - \sigma_{h,k} \cdot F)} \tag{6}$$

$$D_k = G \cdot \sigma_{h,k}{}^{-H} \tag{7}$$

Through a minimisation of the least square differences the constant parameters in Equations 6 and 7 are calibrated over the domain of Switzerland and using daily data from the period September to May 1971-2005 leading to values of E=1.148336, F=0.000966 m^{-1}, G=143.84113 $°C^{-1}$ and H=0.8769335. Note that σ_h is sensitive to the resolution of the two grids to be compared (cf. Eq. 5). It is a measure for the uniformity of the underlying topography and has been computed based on the high-resolution GTOPO30 digital elevation model (https://lta.cr.usgs.gov/GTOPO30) aggregated to a regular grid of 1.25 arc seconds (about 2 km) which reflects the spatial resolution of the observed temperature and precipitation grids (cf. Sec. 2.1). Small values of σ_h indicate a low subgrid-scale topographic variability, such as in the Swiss low-lands, while high values result from non-uniform elevation distributions, such as in areas of inner Alpine valleys. σ_h as derived from GTOPO30 might be different from the subgrid-scale topographic variance employed by the climate models themselves, which is however not relevant here as only grid cell-averaged model output is analysed while σ_h is regarded as a proper estimate of subgrid-scale variability.

Figure S1 (panel c) provides an example of the relation between daily mean temperature and daily snow fraction f_s for grid cells with topographical standard deviations of 50 m and 500 m, respectively. The snowfall amount S_{RI} for a particular day and a particular coarse grid box is finally obtained by multiplying the corresponding $f_{s,RI}$ and P values. A comparison with the *Subgrid method* yields very similar results. For both indices S_{mean} and $S_{q99,}$ mean ratios across all elevation intervals are close to 1 (Fig. 2). At single grid points, maximum deviations are not larger than 1±0.1. Note that for this comparison calibration and validation period are identical (EVAL period). Based on this analysis, it has been decided to separate snowfall according to the *Richards method* throughout this work in both the observations and in the RCMs. The observation-based snowfall estimate obtained by applying the *Richards method* to the observational temperature and precipitation grids after spatial aggregation to the 0.11° RCM resolution will serve as reference for the RCM bias adjustment and will be termed *reference* hereafter. One needs to bear in mind that the parameters C and D of the Richards method were fitted for the Swiss domain only and were later on applied to the entire Alpine domain (cf. Fig. 1).

2.6 Bias adjustment approach

Previous work has revealed partly substantial temperature and precipitation biases of the EURO-CORDEX RCMs over the Alps (e.g. Kotlarski et al., 2014; Smiatek et al., 2016), and one has to expect that the separated snowfall amounts are biased too. This would especially hamper the interpretation of absolute climate change signals of the considered snow indices. We therefore explore possibilities to bias-adjust the simulated snowfall amounts and to directly integrate this bias adjustment into the snowfall separation framework of Section 2.5. Note that we deliberately employ the term *bias adjustment* as opposed to *bias correction* to make clear that only certain aspects of the snowfall climate are adjusted and that the resulting dataset might be subject to remaining inaccuracies.

A simple two-step approach that separately accounts for precipitation and temperature biases and their respective influence on snowfall is chosen. The separate consideration of temperature and precipitation biases allows for a more physically-based bias adjustment of snowfall amounts: Due to the temperature dependency of snowfall occurrence, snowfall biases of a given climate model cannot be expected to remain constant under changing climate conditions. For instance, a climate model with a given temperature bias might pass the snow-rain temperature threshold earlier or later than reality during the general warming process. Hence, traditional bias adjustment approaches based only on a comparison of observed and simulated snowfall amounts in the historical climate would possibly fail due to a non-stationary bias structure. The bias adjustment is calibrated in the EVAL period for each individual GCM-RCM chain and over the region of Switzerland, and is then applied to both the CTRL and SCEN period of each chain and for the entire Alpine domain. To be consistent in terms of horizontal grid spacing, the observational data sets RhiresD and TabsD (see Sec. 2.1) are conservatively regridded to the RCM resolution beforehand.

In a first step, total simulated precipitation is~~was~~ adjusted by introducing an elevation-dependent adjustment factor which adjusts precipitation biases regardless of temperature. For this purpose, mean precipitation ratios (RCM simulation divided by observational analysis) for 250 m elevation intervals ~~were~~ are calculated (Fig. S3). An almost linear relationship of these ratios with elevation ~~was~~ is found. Thus, a linear regression between the intervals from 250 m a.s.l. to 2750 m a.s.l. ~~was~~ is used for each model chain separately to estimate a robust adjustment factor. As the number of both RCM grid points and measurement stations at very high elevations (>2750 m a.s.l.) is small (Sec. 2.1; Fig. S2) and biases are subject to a considerable sampling uncertainty, these elevations ~~were~~ are not considered in the regression. Overall the fits are surprisingly precise except for the altitude bins above 2000 m (Fig. S3). The precipitation adjustment factors (P_{AF}) for a given elevation ~~were~~ are then obtained as the inverse of the fitted precipitation ratios. Multiplying simulated precipitation P with P_{AF} for the respective model chain and elevation results in the adjusted precipitation:

$$\boldsymbol{P_{adj}} = \boldsymbol{P} \cdot \boldsymbol{P_{AF}} \tag{8}$$

For a given GCM-RCM chain and for each elevation interval, the spatially and temporally averaged corrected total precipitation P_{adj} approximately corresponds to the observation-based estimate in the EVAL period.

In the second step of the bias adjustment procedure, temperature biases are accounted for. For this purpose the initial snow fractionation temperature T*=2°C of the Richards separation method (see Sec 2.5) is shifted to the value T^*_a for which the spatially (Swiss domain) and temporally (September to May) averaged simulated snowfall amounts for elevations below 2750 m a.s.l. match the respective observation-based reference (see above). Compared to the adjustment of total precipitation, T^*_a is chosen independent of elevation but separately for each GCM-RCM chain, in order to avoid over-parameterization and to not over-interpret the elevation dependency of mean snowfall in the snowfall reference grid. After this second step of the bias adjustment, the spatially and temporally averaged simulated snowfall amounts below 2750 m a.s.l. match the reference by definition. Hence, the employed simple bias adjustment procedure adjusts domain-mean snowfall biases averaged over the entire season from September to May. It does, however, not correct for biases in the spatial snowfall pattern, in the seasonal cycle, or in the temporal distribution of daily values. Note that, as the underlying high-resolution data sets are available over Switzerland only, the calibration of the bias adjustment methodology is correspondingly restricted, but the adjustment is then applied to the whole Alpine domain. This approach is justified as elevation-dependent mean winter precipitation and temperature biases of the RCMs employed -– assessed by comparison against the coarser-resolved EOBS reference dataset (Haylock et al., 2008) - are very similar for Switzerland and for the entire Alpine analysis domain (Figs. S4 and S5).

3 Evaluation

3.1 RCM raw snowfall

We first carry out an illustrative comparison of RCM raw snowfall amounts (for those simulations only that directly provide snowfall flux) against station observations of snowfall in order to determine whether the simulated RCM snowfall climate contains valid information despite systematic biases. To this end, simulated raw snowfall amounts of seven EURO-CORDEX simulations of the reduced set (Tab. 1) averaged over 250 m-elevation intervals and over the range 950 – 1650 m a.s.l. are compared against observations of measured fresh snow sums from 29 MeteoSwiss stations (Sec. 2.1).. For this purpose a mean snow density of 100 kg/m^3 for the conversion from measured snow depth to water equivalent is assumed. Note that this simple validation is subject to considerable uncertainties as it does not explicitly correct for the scale and elevation gap between grid-cell based RCM output and single-site observations. Especially in complex terrain and for exposed sites, point measurements of snow depth might be non-representative for larger-scale conditions (e.g., Grünewald and Lehning, 2015). Also, the conversion from snow depth to snow water equivalent is of approximate nature only, and fresh snow sums might furthermore misrepresent true snowfall in case that snow melt or snow drift occurs between two snow depth readings.

At low elevations simulated mean September-May raw snowfall sums match the observations well while differences are larger aloft (Fig. 3a). The positive bias at high elevations might arise from the fact that (the very few) observations were made at specific locations while simulated grid point values of the corresponding elevation interval might be located in different areas of Switzerland. It might also be explained by positive RCM precipitation and negative RCM temperature biases at high elevations of the Alps (e.g., Kotlarski et al., 2015). Also note that, in general, the total high-elevation area of the Alpine analysis domain is small and elevations above 2500 m represent less than 5% of the total area (Fig. S2). Both model-based and observation-based estimates for high-elevations are hence subject to a considerable sampling uncertainty and are likely to be less robust than estimates for lower elevations.

At lower elevations, the station network is geographically more balanced and the observations are probably more representative of the respective elevation interval. Despite a clear positive snowfall bias in mid-winter, the RCMs are generally able to reproduce the mean seasonal cycle of snowfall for elevations between 950 m a.s.l. - 1650 m a.s.l. (Fig. 3b). The fact that the major patterns of both the snowfall-elevation relationship and the mean seasonal snowfall cycle are well represented indicates the general and physically consistent applicability of RCM output to assess future changes in mean and heavy Alpine snowfall. However, substantial biases in snowfall amounts are apparent and a bias adjustment of simulated snowfall seems to be required prior to the analysis of climate change signals of individual snowfall indices.

3.2 Evaluation of the reference snowfall

The snowfall separation employing the *Richards method* (Sec. 2.5) and, as a consequence, also the bias adjustment (Sec. 2.6) make use of the 2 km reference snowfall grid derived by employing the *Subgrid method* on the observed temperature and precipitation grids. Hence, the final results of this study could to some extent be influenced by inaccuracies and uncertainties of the reference snowfall grid itself. In order to assess the quality of the latter and in absence of a further observation-based reference we here present an approximate evaluation.

First, the reference snowfall grid is evaluated against fresh snow sums at the 29 Swiss stations that ~~were~~ are also used for evaluating RCM raw snowfall. Note the limitations of such a comparison as outlined in Chapter 3.1. The comparison of black and red markers and lines in Figure 3 indicates a good agreement of mean snowfall at individual elevation intervals (left panel) as well for the mean annual cycle of snowfall at medium elevations (right panel). The reference snowfall grid is obviously a good approximation of site-scale fresh snow sums. Note that similarly to the RCM raw snowfall evaluation, all 2 km reference snowfall grid cells in the respective elevation interval are considered. The good agreement, however, still holds if only those 2 km grid cells covering the 29 site locations are considered (not shown here).

Second, both the 2 km reference snowfall grid and the 0.11° reference snowfall grid obtained by employing the Richards method to aggregated temperature and precipitation values (Sec. 2.5) are compared against the gridded HISTALP dataset of solid precipitation (Chimani et al., 2011). The latter is provided at a monthly resolution on a 5' grid covering the Greater Alpine Region. It is based on monthly snowfall fraction estimates that are used to scale a gridded dataset of total precipitation. The comparison of the three datasets for the region of Switzerland (for which the 2 km reference snowfall is available) in the EVAL period 1971-2005 yields an approximate agreement of both the magnitude of mean winter snowfall and its spatial pattern (Fig. S6). The three data sets differ with respect to their spatial resolution but all show a clear dependency of snowfall on topography and mean September-May snowfall sums above 1000 mm over most parts of the Alpine ridge. Climatologically warm and dry valleys, on the other hand, are represented by minor snowfall amounts of less than 400 mm only.

As mentioned before these evaluations of the reference snowfall grid are subject to uncertainties and, furthermore, they only cover mean snowfall amounts. However, they provide basic confidence in the applicability of the reference snowfall grid for the purposes of snowfall separation and bias adjustment in the frame of the present study.

3.3 Calibration of bias adjustment

The analysis of total precipitation ratios (RCM simulations with respect to observations) for the EVAL period, which are computed to carry out the first step of the bias adjustment procedure, reveals substantial elevation dependencies. All simulations tend to overestimate total precipitation at high elevations (Fig. S3). This fact might ultimately be connected to an overestimation of surface snow amount in several EURO-CORDEX RCMs as reported by Terzago et al. (2017). As the precipitation ratio between simulations and observations depends approximately linearly on elevation, the calculation of P_{AF} via a linear regression of the ratios against elevation (see Sec. 2.6) seems reasonable. By taking the inverse of this linear relation, P_{AF} for every model and elevation can be derived. For the CCLM simulations, these correction factors do not vary much with height, while P_{AF} for MPI-ESM - REMO and EC-EARTH - HIRHAM is much larger than 1 in low lying areas, indicating a substantial underestimation of observed precipitation sums (Fig. 4a). However, for most elevations and simulations, P_{AF} is generally smaller than 1, i.e., total precipitation is overestimated by the models. Similar model biases in the winter and spring seasons have already been reported in previous works (e.g., Rajczak et al., 2017; Smiatek et al., 2016). Especially at high elevations, these apparent positive precipitation biases could be related to observational undercatch, i.e., an underestimation of true precipitation sums by the observational analysis. Frei et al. (2003) estimated seasonal Alpine precipitation undercatch for three elevation intervals. Results show that measurement biases are largest in winter and increase with altitude. However, a potential undercatch (with a maximum of around 40% at high elevations in winter; Frei et al., 2003) can only partly explain the often substantial overestimation of precipitation found in the present work.

After applying P_{AF} to the daily precipitation fields, a snowfall fractionation at the initial T^* of 2 °C (see Eq. (4)) would lead to a snowfall excess in all 12 simulations as models typically experience a cold winter temperature bias. To match the observation-based and spatio-temporally averaged reference snowfall below 2750 m a.s.l., T^* for all models needs to be decreased during the second step of the bias adjustment (Fig. 4b). The adjusted T^*_a values indicate a clear positive relation with the mean temperature bias in the EVAL period. This feature is expected since the stronger a particular model's cold bias the stronger the required adjustment of the snow fractionation temperature T^* towards lower values in order to avoid a positive snowfall bias. Various reasons for the scatter around a simple linear relation in Figure 4b can be thought of. These include remaining spatial inaccuracies of the corrected precipitation grid, elevation-dependent temperature biases and misrepresented temperature-precipitation relationships at daily scale. Note that precipitation and temperature biases heavily depend on the GCM-RCM chain and seem to be rather independent from each other. Concerning the partly substantial temperature biases of the EURO-CORDEX models shown in Figure 4b, their magnitude largely agrees with Kotlarski et al. (2014; in reanalysis-driven simulations) and Smiatek et al. (2016).

3.4 Evaluation of snowfall indices

We next assess the performance of the bias adjustment procedure by comparing snowfall indices derived from separated and bias-adjusted RCM snowfall amounts against the observation-based reference. The period for which this comparison is carried out is EVAL, i.e., it is identical to the calibration period of the bias adjustment. We hence do not intend a classical cross validation exercise with separate calibration and validation periods, but try to answer the following two questions: (a) Which aspects of the Alpine snowfall climate are adjusted, and (b) for which aspects do biases remain even after application of the bias adjustment procedure.

Figure 5 shows the evaluation results of the six snowfall indices based on the separated and not bias-adjusted simulated snowfall ($RCM_{sep+nba}$), and the separated and bias-adjusted simulated snowfall (RCM_{sep+ba}). In the first case the snowfall separation of raw precipitation is performed with T*=2°C, while in the second case precipitation is adjusted and the separation is performed with a bias-adjusted temperature T^*_a. The first column represents the mean September to May statistics, while columns 2-4 depict the seasonal cycle at monthly resolution for three distinct elevation intervals.

The analysis of S_{mean} confirms that RCM_{sep+ba} is able to reproduce the observation-based reference in the domain mean as well as in most individual elevation intervals. The domain-mean agreement is a direct consequence of the design of the bias adjustment procedure (see above). $RCM_{sep+nba}$, on the other hand, consistently overestimates S_{mean} by up to a factor of 2.5 as a consequence of positive precipitation and negative temperature biases (cf. Fig. 4). Also the seasonal cycle of S_{mean} for RCM_{sep+ba} yields a satisfying performance across all three elevation intervals, while $RCM_{sep+nba}$ tends to produce too much snowfall over all months and reveals an increasing model spread with elevation.

For the full domain and elevations around 1000 m, the observation-based reference indicates a mean S_{freq} of 20% between September and May. Up to 1000 m a.s.l. RCM_{sep+ba} reflects the increase of this index with elevation adequately. However, towards higher elevations the approximately constant S_{freq} of 30% in the reference is not captured by the simulation-derived snowfall. Notably during wintertime, both RCM_{sep+ba} and $RCM_{sep+nba}$ produce too many snowfall days, i.e., overestimate snowfall frequency. This feature is related to the fact that climate models typically tend to overestimate the wet day frequency over the Alps especially in wintertime (Rajczak et al., 2013) and that the bias adjustment procedure employed does not explicitly correct for potential biases in precipitation frequency. Due to the link between mean snowfall on one side and snowfall frequency and mean intensity on the other side, opposite results are obtained for the mean snowfall intensity S_{int}. RCM_{sep+ba} largely underestimates mean intensities during snowfall days while $RCM_{sep+nba}$ typically better reflects the reference. Nevertheless, deviations during winter months at mid-elevations are not negligible. Mean September-May S_{frac} in the reference exponentially increases with elevation. This behaviour is reproduced by both RCM_{sep+ba} and $RCM_{sep+nba}$. Notwithstanding, RCM_{sep+ba} results are more accurate compared to $RCM_{sep+nba}$, which turns out to be biased towards too large snowfall fractions.

For the two heavy snowfall indices S_{q99} and S_{1d}, $RCM_{sep+nba}$ appears to typically match the reference better than RCM_{sep+ba}. Especially at high elevations, RCM_{sep+ba} produces too low snowfall amounts. This again illustrates the fact that the bias adjustment procedure is designed to adjust biases in mean snowfall, but does not necessarily improve further aspects of the simulated snowfall climate.

The spatial patterns of S_{mean} for the 12 RCM_{sep+ba} simulations from September to May are presented in Figure 6. The observational-based reference (~~bottom~~ lower-right panel) reveals a snowfall distribution with highest values along the Alpine main ridge, whereas the Swiss plateau, Southern Ticino and main valleys such as the Rhône and Rhine valley experience less snowfall. Almost all bias-adjusted models are able to represent the overall picture with snow-poor lowlands and snow-rich Alpine regions. Nevertheless substantial differences to the observations concerning the spatial snowfall pattern can arise. EC-EARTH - HIRHAM, for example, is subject to a noisy structure. This could be the result of frequent grid-cell storms connected to parameterisations struggling with complex topographies. Such inaccuracies in the spatial pattern are not corrected for by our simple bias adjustment approach which only targets domain-mean snowfall amounts at elevations below 2750 m a.s.l. and that does not considerably modify the simulated spatial snowfall patterns.. Note that these patterns are obviously strongly determined by the RCM itself and only slightly depend on the driving GCM (see, for instance, the good agreement among the CCLM and the RCA simulations).

In summary, after applying the bias adjustment to the simulations most snowfall indices are fairly well represented at elevations below 1000 m a.s.l.. With increasing altitude and smaller sample sizes in terms of number of grid cells, reference and RCM_{sep+ba} diverge. This might be caused by the remaining simulated overestimation of S_{freq} and an underestimation of S_{int}. While the bias adjustment approach leads to a reduction of S_{int} due to the total precipitation adjustment, S_{freq} is only slightly modified by this correction and by the adjustment of T^*. Nevertheless, these two parameters strongly influence other snowfall indices. The counteracting effects of overestimated S_{freq} and underestimated S_{int} result in appropriate amounts of S_{mean} whereas discrepancies for S_{q99} and S_{1d} are mainly driven by the underestimation of S_{int}.

4 Snowfall projections for the late 21st century

For the study of climate change signals, the analysis domain is extended to the entire Alps (see Sec. 2.3). Due to the identified difficulties of bias-adjusting certain snowfall indices (see Sec 3.4), emphasis is laid ~~upon~~ on relative signals of change (see Eq. 2). This type of change can be expected to be less dependent on the remaining inaccuracies after the adjustment. If not stated otherwise, all results in this Section are based on the RCM_{sep+ba} data, i.e., on separated and bias-adjusted RCM snowfall, and on the RCP8.5 emission scenario. Depending on the type of analysis, either the full or the reduced model set is used (see Tab. 1 and Supplementary Material, Part B).

Projections for seasonal S_{mean} show a considerable decrease over the entire Alpine domain (Fig. 7). Most RCMs project largest percentage losses of more than 80% across the Alpine forelands and especially in its topographic depressions such as the Po and Rhone valleys. Over the Alpine ridge, reductions are smaller but still mostly negative. Elevated regions between Southeastern Switzerland, Northern Italy and Austria seem to be least affected by the overall snowfall reduction. Some of the simulations (e.g., CNRM-RCA, MPI-ESM-RCA or MPI-ESM-REMO) project only minor changes in these regions. Experiments employing the same RCM but different driving GCMs (e.g. the four simulations of RCA), but also experiments employing the same GCM but different RCMs (e.g. the

~~three~~ four simulations driven by EC-EARTH, though different realizations) can significantly disagree in regional-scale change patterns and especially in the general magnitude of change. This highlights a strong influence of both the driving GCMs and the RCMs themselves on snowfall changes, representing effects of large-scale circulation and meso-scale response, respectively.

A more detailed analysis is provided in Fig. 8 which addresses the vertical and seasonal distribution of snowfall changes. It reveals that relative (seasonal mean) changes of S_{mean} appear to be strongly dependent on elevation (Fig.8, top left panel). The multi-model mean change ranges from -80% at low elevations to -10% above 3000 m a.s.l.. Largest differences between neighbouring elevation intervals are obtained from 750 m a.s.l. to 1500 m a.s.l.. Over the entire Alps, the results show a reduction of S_{mean} by -35% to -55% with a multi-model mean of -45%. The multi-model spread appears to be rather independent of elevation and is comparably small, confirming that, overall, the spatial distribution~~s~~ of the change pattern~~s are~~ is similar across all model chains (cf. Fig. 7). All simulations point to decreases over the entire nine-month period September to May for the two elevation intervals <1000 m a.s.l. and 1000 to 2000 m a.s.l.. Above 2000 m a.s.l., individual simulations show an increase of S_{mean} by up to 20% in mid-winter which leads to a slightly positive change in the multi-model mean in January and February.

Decreases of S_{freq} are very similar to changes in mean snowfall. Mean September-May changes are largest below 1000 m a.s.l., while differences among elevation intervals become smaller at higher elevations. In-between is a transition zone with rather strong changes with elevation, which approximately corresponds to the mean elevation of the September-May zero-degree line in today's climate (e.g., Ceppi et al., 2012; MeteoSchweiz, 2016). Individual simulations with large reductions in S_{mean}, such as the RCA experiments, also project strongest declines in S_{freq}. In contrast, the mean snowfall intensity S_{int} is subject to smallest percentage variations in our set of snowfall indices. Strong percentage changes for some models in September are due to the small sample size (only few grid points considered) and the low snowfall amounts in this month. Apart from mid elevations with decreases of roughly -10%, mean intensities from September to May are projected to remain almost unchanged by the end of the century. For both seasonal and monthly changes, model agreement is best for high elevations while the multi-model spread is largest for the lowlands. Large model spread at low elevations might be caused by the small number of grid points used for averaging over the respective elevation interval, especially in autumn and spring.

Similar results are obtained for the heavy snowfall indices S_{q99} and S_{1d}. While percentage decreases at lowermost elevations are even larger than for S_{mean}, losses at high elevations are less pronounced, resulting in similar domain-mean change signals for heavy and mean snowfall. Substantial differences between monthly δS_{q99} and δS_{1d} appear at elevations below 1000 m a.s.l.. Here, percentage losses of S_{q99} are typically slightly more pronounced. Above 2000 m a.s.l. both indices appear to remain almost constant between January and March with change signals close to zero. The multi-model mean changes even hint to slight increases of both indices. Concerning changes in the snowfall fraction, i.e., in the relative contribution of snowfall to total precipitation, our results indicate that current seasonal and domain mean S_{frac} might drop by about -50% (Fig. 8, lowermost row). Below 1000 m a.s.l., the strength of the signal is almost independent of the month, and multi-model average changes of the snow fraction of about -80% are obtained. At higher elevations changes during mid-winter are less pronounced compared to autumn and spring but still negative.

5 Discussion

5.1 Effect of temperature, snowfall frequency and intensity on snowfall changes

The results in Section 4 indicate substantial changes of snowfall indices over the Alps in regional climate projections. With complementary analyses presented in Figures 9 and 10 we shed more light on the responsible mechanisms, especially concerning projected changes in mean and heavy snowfall. For this purpose Figures 9a-b,e-f show the relationship of both mean and heavy snowfall amounts in the CTRL period and their respective percentage changes with the climatological CTRL temperature of the respective (climatological) month, elevation interval and GCM-RCM chain. For absolute amounts (S_{mean}, S_{q99}; Fig. 9a,e) a clear negative relation is found, i.e., the higher the CTRL temperature the lower the snowfall amounts. For S_{mean} the relation levels off at mean temperatures higher than about 6°C with mean snowfall amounts close to zero. For temperatures below about -6°C a considerable spread in snowfall amounts is obtained, i.e., mean temperature does not seem to be the controlling factor here. Relative changes of both quantities (Fig. 9b,f), however, are strongly controlled by the CTRL period's temperature level with losses close to 100% for warm climatic settings and partly increasing snowfall amounts for colder climates. This dependency of relative snowfall changes on CTRL temperature is in line with previous works addressing future snowfall changes on both hemispheric and regional scales (de Vries et al., 2014; Krasting et al., 2013; Räisänen, 2016). The spread of changes within a given CTRL temperature bin can presumably be explained by the respective warming magnitudes that differ between elevations, months and GCM-RCM chains. About half of this spread can be attributed to the month and the elevation alone (compare the spread of the black markers to the one of the red markers which indicate multi-model averages).

For most months and elevation intervals, percentage reductions in S_{mean} and S_{q99} reveal an almost linear relationship with δS_{freq} (Fig. 9c, g). The decrease of S_{freq} with future warming can be explained by a shift of the temperature probability distribution towards higher temperatures, leading to fewer days below the freezing level (Fig. 10, top row). Across the three elevation intervals <1000 m a.s.l., 1000-2000 m a.s.l. and > 2000 m a.s.l., relative changes in the number of days with temperatures below the freezing level ($T \leq 0°C$) are in the order of -65%, -40% and -20%, respectively (not shown). This approximately corresponds to the simulated decrease of S_{freq} (cf. Fig 8), which in turn, is of a similar magnitude as found in previous works addressing future snowfall changes in the Alps (Schmucki et al., 2015b; Zubler et al., 2014). Due to the general shift of the temperature distribution and the "loss" of very cold days (Fig. 10, top row) future snowfall furthermore occurs in a narrower temperature range (Fig. 10, second row).

Contrasting this general pattern of frequency-driven decreases of both mean and heavy snowfall, no changes or even slight increases of S_{mean}, S_{q99} and S_{1d} at high elevations are expected in mid-winter (see Fig. 8). This can to some part be explained by the general increase of total winter precipitation

(Rajczak et al., 2017; Smiatek et al., 2016) that obviously offsets the warming effect in high-elevation regions where a substantial fraction of the future temperature PDF is still located below the rain-snow transition (Fig. 10, top row). This process has also been identified in previous works to be, at last partly, responsible for future snowfall increases (de Vries et al., 2014; Krasting et al., 2013; Räisänen, 2016). Furthermore, the magnitude of the increases of both mean and heavy snowfall is obviously driven by positive changes of S_{int}, while S_{freq} remains constant (Fig. 9c,g). An almost linear relationship between positive changes of S_{int} and positive changes of S_{mean} and S_{q99} is obtained (Fig. 9d,h; upper right quadrants. Nevertheless, the high-elevation mid-winter growth in S_{mean} is smaller than the identified increases of mean winter total precipitation. This can be explained by the persistent decrease of S_{frac} during the cold season (see Fig. 8, lowermost row).

For elevation intervals with simulated monthly temperatures between -6°C and 0°C in the CTRL period, S_{mean} appears to decrease stronger than S_{q99} (cf. Fig. 9b,f). O'Gorman (2014) found a very similar behaviour when analysing mean and extreme snowfall projections over the Northern Hemisphere within a set of GCMs. This finding is related to the fact that future snowfall decreases are mainly governed by a decrease of snowfall frequency while snowfall increases in high-elevated regions in mid-winter seem to be caused by increases of snowfall intensity. It can obviously be explained by the insensitivity of the temperature interval at which extreme snowfall occurs to climate warming and by the shape of the temperature – snowfall intensity distribution itself (Fig. 10, third row). The likely reason behind positive changes of S_{int} at high-elevated and cold regions is the higher water holding capacity of the atmosphere in a warmer climate. According to the Clausius-Clapeyron relation, saturation vapour pressure increases by about 7% per degree warming (Held and Soden, 2006). Previous studies have shown that simulated changes of heavy and extreme precipitation on daily time scales are consistent with this theory (e.g., Allen and Ingram, 2002; Rajczak et al., 2017). In terms of snowfall, we find the Clausius-Clapeyron relation to be applicable for negative temperatures up to approximately -5°C as well (Fig. 10, third row, dashed lines). Inconsistencies for temperatures between -5°C and 0°C are due to a snow fraction *sf* < 100% for corresponding precipitation events.

For further clarification, Figure 11 schematically illustrates the governing processes behind the changes of mean and heavy snowfall that differ between climatologically warm (decreasing snowfall) and climatologically cold climates (increasing snowfall). As shown in Figure 10 (third row), the mean S_{int} distribution is rather independent on future warming and similar temperatures are associated with similar mean snowfall intensities. In particular, heaviest snowfall is expected to occur slightly below the freezing level in both the CTRL and the SCEN period (Fig. 11a). How often do such conditions prevail in the two periods? In a warm current climate, i.e., at low elevations or in the transition seasons, heavy snowfall only rarely occurs as the temperature interval for highest snowfall intensity is already situated in the left tail of the CTRL period's temperature distribution (Fig. 11b). With future warming, i.e., with a shift of the temperature distribution to the right, the probability for days to occur in the heavy snowfall temperature interval (dark grey shading) decreases stronger than the probability of days to occur in the overall snowfall regime (light grey shading). This results in (1) a general decrease of snowfall frequency, (2) a general decrease of mean snowfall intensity and (3) a general and similar decrease of both mean and heavy snowfall amounts. In contrast, at cold and high-elevated sites CTRL period temperatures are often too low to trigger heavy snowfall since a substantial fraction of the temperature PDF is located to the left of the heavy snowfall temperature interval (Fig. 11 c). The shifted distribution in a warmer SCEN climate, however, peaks within the temperature interval that favours heavy snowfall. This leads to a probability increase for days to occur in the heavy snowfall temperature range despite the general reduction in S_{freq} (lower overall probability of days to occur in the entire snowfall regime, light grey). As a consequence, mean S_{int} tends to increase and the reduction of heavy snowfall amounts is less pronounced (or even of opposing sign) than the reduction in mean snowfall. For individual (climatologically cold) regions and seasons, the increase of mean S_{int} might even compensate the S_{freq} decrease, resulting in an increase of both mean and heavy snowfall amounts. Note that in a strict sense these explanations only hold in the case that the probability of snowfall to occur at a given temperature does not change considerably between the CTRL and the SCEN period. This behaviour is approximately found (Fig. 10, bottom row), which presumably indicates only minor contributions of large scale circulation changes and associated humidity changes on both the temperature - snowfall frequency and the temperature - snowfall intensity relation.

5.2 Emission scenario uncertainty

The projections presented in the previous sections are based on the RCP8.5 emission scenario, but will depend on the specific scenario considered. To assess this ~~type of~~ uncertainty we here compare the RCM_{sep+ba} simulations for the previously shown RCP8.5 emission scenario against those assuming the more moderate RCP4.5 scenario. As a general picture, the weaker RCP4.5 scenario is associated with less pronounced changes of snowfall indices (Fig. 12). Differences in mean seasonal δS_{mean} between the two emission scenarios are most pronounced below 1000 m a.s.l. where percentage changes for RCP4.5 are about one third smaller than for RCP8.5. At higher elevations, multi-model mean changes better agree and the multi-model ranges for the two emission scenarios start overlapping, i.e., individual RCP4.5 experiments can be located in the RCP8.5 multi-model range and vice versa. Over the entire Alpine domain, about -25% of current snowfall is expected to be lost under the moderate RCP4.5 emission scenario while a reduction of approximately -45% is projected for RCP8.5. For seasonal cycles, the difference of δS_{mean} between RCP4.5 and RCP8.5 is similar for most months and slightly decreases with altitude. Above 2000 m a.s.l., the simulated increase of S_{mean} appears to be independent of the chosen RCP in January and February, while negative changes before and after mid-winter are more pronounced for RCP8.5. Alpine domain mean δS_{q99} almost doubles under the assumption of stronger GHG emissions. This is mainly due to differences at low elevations whereas above 2000 m a.s.l. δS_{q99} does not seem to be strongly affected by the choice of the emission scenario. Differences in monthly mean changes are in close analogy to δS_{mean}. Higher emissions lead to a further negative shift in δS_{q99}. Up to mid-elevations differences are rather independent of the season. However, at highest elevations and from January to March, differences between RCP4.5 and RCP8.5 are very small.

Despite the close agreement of mid-winter snowfall increases at high elevations between the two emission scenarios, obvious differences in the spatial extent of the region of mean seasonal snowfall increases can be found (cf Figs. S7 and 7 for δS_{mean}, and Figs. S8 and S9 for δS_{q99}). In most simulations, the number of grid cells along the main Alpine ridge that show either little change or even increases of seasonal mean S_{mean} or S_{q99} is larger for RCP4.5 than for RCP8.5 with its larger warming magnitude.

5.3 Intercomparison of projections with separated and raw snowfall

The snowfall projections presented above are based on the RCM_{sep+ba} data set, i.e. on separated and bias-adjusted snowfall amounts. To assess the robustness of these estimates we here compare the obtained change signals against the respective signals based on $RCM_{sep+nba}$ (separated and not bias-adjusted) and simulated raw snowfall output (RCM_{raw}). This comparison is restricted to the seven RCMs providing raw snowfall as output variable (see Tab. 1).

The three different change estimates agree well with each other in terms of relative snowfall change signals (Fig. 13, top row). Multi-model mean relative changes are very similar for all analysed snowfall indices and elevation intervals. In many cases, separated and not bias-adjusted snowfall ($RCM_{sep+nba}$) is subject to slightly smaller percentage decreases. Multi-model mean differences between RCM_{sep+ba}, $RCM_{sep+nba}$ and RCM_{raw} simulations are smaller than the corresponding multi-model spread of RCM_{sep+ba} simulations and emission scenario uncertainties (cf. Figs. 12, 13 and S10). This agreement in terms of relative change signals is in contrast to absolute change characteristics (Fig. 13, bottom row). Results based on the three data sets agree in the sign of change, but not in their magnitude, especially at high elevations >2000 m a.s.l.. As the relative changes are almost identical, the absolute changes strongly depend upon the treatment of biases in the control climate.

In summary, these findings indicate that (a) the snowfall separation method developed in the present work yields rather good proxies for relative changes of snowfall indices in raw RCM output (which is not available for all GCM-RCM chains), and that (b) the additional bias adjustment of separated snowfall amounts only has a weak influence on relative change signals of snowfall indices, but can have substantial effects on absolute changes.

6 Conclusions and outlook

The present work makes use of state-of-the-art EURO-CORDEX RCM simulations to assess changes of snowfall indices over the European Alps by the end of the 21st century. For this purpose, snowfall is separated from total precipitation using near-surface air temperature in both the RCMs and in the observation-based estimate on a daily basis. The analysis yields a number of robust signals, consistent across a range of climate model chains and across emission scenarios. Relating to the main objectives we find the following:

Snowfall separation on the RCM grid. Binary snow fractionation with a fixed temperature threshold on coarse-resolution grids (with 11 km resolution) leads to an underestimation of mean snowfall and an overestimation of heavy snowfall. To overcome these deficiencies, the Richards snow fractionation method is implemented. This approach expresses that the coarse-grid snow fraction depends not only on daily mean temperature, but also on topographical subgrid-scale variations. Accounting for the latter results in better estimates for mean and heavy snowfall. However, due to limited observational coverage the parameters of this method are fitted for Switzerland only and are then applied to the entire Alpine domain. Whether this spatial transfer is robust could further be investigated by using observational data sets covering the full domain of interest but is out of the scope of this study.

Snowfall bias adjustment. Simulations of the current EURO-CORDEX ensemble are subject to considerable biases in precipitation and temperature, which translate into biased snowfall amounts. In the EVAL period, simulated precipitation is largely overestimated, with increasing biases toward higher altitudes. On the other hand, simulated near surface temperatures are generally too low with largest deviations over mountainous regions. These findings were already reported in previous studies for both the current EURO-CORDEX data set but also for previous RCM ensembles (e.g. Frei et al., 2003; Kotlarski et al., 2012; Kotlarski et al., 2015; Rajczak et al., 2013; Smiatek et al., 2016). By implementing a simple bias adjustment approach, we are able to partly reduce these biases and the associated model spread, which should enable more robust change estimates. The adjusted model results reproduce the seasonal cycles of mean snowfall fairly well. However, substantial biases remain in terms of heavy snowfall, snowfall intensities (which in general are overestimated), snowfall frequencies, and spatial snowfall distributions. Further improvements might be feasible by using more sophisticated bias adjustment methods, such as quantile mapping (e.g., Rajczak et al., 2016), local intensity scaling of precipitation (e.g., Schmidli et al., 2006), or weather generators (e.g. Keller at al., 2016). Advantages of the approach employed here are its simplicity, its direct linkage to the snowfall separation method and, as a consequence, its potential ability to account for non-stationary snowfall biases. Furthermore, a comparison to simulated raw snowfall for a subset of seven simulations revealed that relative change signals are almost independent of the chosen post-processing strategy.

Snowfall projections for the late 21st century. Snowfall climate change signals are assessed by deriving the changes in snowfall indices between the CTRL period 1981 - 2010 and the SCEN period 2070 - 2099. Our results show that by the end of the 21st century, snowfall over the Alps will be considerably reduced. Between September and May mean snowfall is expected to decrease by approximately -45% (multi-model mean) under an RCP8.5 emission scenario. For the more moderate RCP4.5 scenario, multi-model mean projections show a decline of -25%. These results are in good agreement with previous works (e.g. de Vries et al., 2014; Piazza et al., 2014, Räisänen, 2016). Low-lying areas experience the largest percentage changes of more than -80%, while the highest Alpine regions are only weakly affected. Variations of heavy snowfall, defined by the 99% all-day snowfall percentile, show an even more pronounced signal at low-lying elevations. With increasing elevation, percentage changes of heavy snowfall are generally smaller than for mean snowfall. O'Gorman (2014) found a very similar behaviour by analysing projected changes in mean and extreme snowfall over the entire Northern Hemisphere. He pointed out that heavy and extreme snowfall occurs near an optimal temperature (near or below freezing, but not too cold), which seems to be independent of climate warming. We here confirm this finding. At mid and high elevations heavy snowfall in a warmer climate will still occur in the optimal temperature range, hence, heavy snowfall amounts will decrease less strongly compared to mean snowfall, and may even increase in some areas.

At first approximation, the magnitude of future warming strongly influences the reduction of mean and heavy snowfall by modifying the snowfall frequency. Snowfall increases may however occur at high (and thus cold) elevations, and these are not caused by frequency changes. Here, snowfall increases due to (a) a general increase of total winter precipitation combined with only minor changes in snowfall frequency, and (b) more intense snowfall. This effect has a pronounced altitudinal distribution and may be particularly strong under conditions (depending upon location and season) where the current climate is well below freezing. With the expected warming a shift towards a temperature range more favourable to snowfall (near or below freezing, but not too cold) can be expected with corresponding increases of mean snowfall, despite a general decrease of the snowfall fraction.

Note that individual EURO-CORDEX experiments were completely or partly omitted from our analysis (see Supplementary Material, Part B and Table 1). However, when comparing the ensemble results based on the reduced and the full model set only slight differences are found and our main results and conclusions do not change (compare Figure 12 to Figure S15). This indicates a robust ensemble analysis that is only little affected by potentially critical shortcomings of individual simulations.

The identified future changes of snowfall over the Alps can lead to a variety of impacts in different sectors. With decreasing snowfall frequencies and the general increase of the snowline (e.g., Beniston, 2003; Gobiet et al., 2014; Hantel et al., 2012), both associated with temperature changes, ski lift operators are looking into an uncertain future. A shorter snowfall season will likely put them under greater financial pressure. Climate change effects might be manageable only for ski areas reaching up to high elevations (e.g. Elsasser and Bürki, 2002). Even so these resorts might start later into the ski season, the snow conditions into early spring could change less dramatically due to projected high-elevation snowfall increases in mid-winter. A positive aspect of the projected decrease in snowfall frequency might be a reduced expenditures for airport and road safety (e.g., Zubler et al., 2015).

At lower altitudes, an intensification of winter precipitation, combined with smaller snowfall fractions (Serquet et al., 2013), increases the flood potential (Beniston, 2012). Snow can act as a buffer by releasing melt water constantly over a longer period of time. With climate warming, this storage capacity is lost, and heavy precipitation immediately drains into streams and rivers which might not be able to take up the vast amount of water fast enough. Less snowmelt will also have impacts on hydropower generation and water management (e.g., Weingartner et al., 2013). So far, many Alpine regions are able to bypass dry periods by tapping melt water from mountainous regions. With reduced snow-packs due to less snowfall, water shortage might become a serious problem in some areas.

Regarding specific socio-economic impacts caused by extreme snowfall events, conclusions based on the results presented in this study are difficult to draw. It might be possible that the 99% all-day snowfall percentile we used for defining heavy snowfalls, is not appropriate to speculate about future evolutions of (very) rare events (Schär et al., 2016). To do so, one might consider applying a generalized extreme value (GEV) analysis which is more suitable for answering questions related to rare extreme events.

7 Data Availability

The EURO-CORDEX RCM data analysed in the present work are publicly available - parts of them for non-commercial use only - via the Earth System Grid Federation archive (ESGF; e.g., https://esgf-data.dkrz.de). The observational datasets RHiresD and TabsD as well as the snow depth data for Switzerland are available for research and educational purposes from kundendienst@meteoschweiz.ch. The analysis code is available from the corresponding author on request.

8 Competing Interests

The authors declare that they have no conflict of interest.

9 Acknowledgements

We gratefully acknowledge the support of Jan Rajczak, Urs Beyerle and Curdin Spirig (ETH Zurich) as well as Elias Zubler (MeteoSwiss) in data acquisition and pre-processing. Christoph Frei (MeteoSwiss) and Christoph Marty (WSL-SLF) provided important input on specific aspects of the analysis. The GTOPO30 digital elevation model is available from the U.S. Geological Survey. Finally, we thank the climate modelling groups of the EURO-CORDEX initiative for producing and making available their model output.

10 References

Abegg, B. A., S., Crick, F., and de Montfalcon, A.: Climate change impacts and adaptation in winter tourism, in: Climate change in the European Alps: adapting winter tourism and natural hazards management, edited by: Agrawala, S., Organisation for Economic Cooperation and Development (OECD), Paris, France, 25-125, 2007.

Allen, M. R., and Ingram, W. J.: Constraints on future changes in climate and the hydrologic cycle, Nature, 419, 224-232, 10.1038/nature01092, 2002.

Beniston, M.: Climatic Change in Mountain Regions: A Review of Possible Impacts. Clim Change, 59, 5-31.

Beniston, M.: Impacts of climatic change on water and associated economic activities in the Swiss Alps, J Hydrol, 412, 291-296, 10.1016/j.jhydrol.2010.06.046, 2012.

Ceppi, P., Scherrer, S.C., Fischer, A.M., and Appenzeller, C.: Revisiting Swiss temperature trends 1959–2008, Int J Climatol, 32, 203-213, 10.1002/joc.2260, 2012.

CH2011: Swiss Climate Change Scenarios CH2011, published by C2SM, MeteoSwiss, ETH, NCCR Climate, and OcCC, Zurich, Switzerland, 88 pp, 2011.

Chimani, B., Böhm, R., Matulla, C., and Ganekind, M.: Development of a longterm dataset of solid/liquid precipitation, Adv Sci Res, 6, 39-43, 10.5194/asr-6-39-2011, 2011.

de Vries, H., Haarsma, R. J., Hazeleger, W.: On the future reduction of snowfall in western and central Europe. Clim Dyn, 41, 2319-2330, 10.1007/s00382-012-1583-x, 2013.

de Vries, H., Lenderink, G., and van Meijgaard, E.: Future snowfall in western and central Europe projected with a high-resolution regional climate model ensemble, Geophys Res Lett, 41, 4294-4299, 10.1002/2014GL059724, 2014.

Deser, C., Knutti, R., Solomon, S. and Phillips, A. S.: Communication of the role of natural variability in future North American climate. Nature Clim Change, 2, 775-779, 2012.

Elsasser, H. and Bürki, R.: Climate change as a threat to tourism in the Alps. Climate Research, 20, 253-257.

Fischer, A. M., Keller, D. E., Liniger, M. A., Rajczak, J., Schär, C., and Appenzeller, C.: Projected changes in precipitation intensity and frequency in Switzerland: a multi-model perspective, Int J Climatol, 35, 3204-3219, 10.1002/joc.4162, 2015.

Fischer, E. M. and Knutti, R.: Observed heavy precipitation increase confirms theory and early models. Nature Clim Change, 6, 986-992, 10.1038/NCLIMATE3110, 2016.

Frei, C. and Schär, C.: A precipitation climatology of the Alps from high-resolution rain-gauge observations, Int J Climatol, 18, 873-900, 10.1002/(Sici)1097-0088(19980630)18:8<873::Aid-Joc255>3.0.Co;2-9, 1998.

Frei, C., Christensen, J. H., Déqué, M., Jacob, D., Jones, R. G., and Vidale, P. L.: Daily precipitation statistics in regional climate models: Evaluation and intercomparison for the European Alps, J Geophys Res-Atmos, 108, 10.1029/2002jd002287, 2003.

Frei, C.: Interpolation of temperature in a mountainous region using nonlinear profiles and non-Euclidean distances, Int J Climatol, 34, 1585-1605, 10.1002/joc.3786, 2014.

Giorgi, F.: Simulation of regional climate using a limited area model nested in a general circulation model, J Climate, 3, 941-963, 1990.

Giorgi, F., Jones, C., and Asrar, G. R.: Addressing climate information needs at the regional level: the CORDEX framework, World Meteorological Organization (WMO) Bulletin, 58, 175, 2009.

Giorgi, F., Torma, C., Coppola, E., Ban, N., Schär, C., and Somot, S.: Enhanced summer convective rainfall at Alpine high elevations in response to climate warming, Nat Geo, 9, 584-589, 10.1038/ngeo2761, 2016.

Gobiet, A., Kotlarski, S., Beniston, M., Heinrich, G., Rajczak, J., and Stoffel, M.: 21st century climate change in the European Alps - A review, Science of the Total Environment, 493, 1138-1151, 10.1016/j.scitotenv.2013.07.050, 2014.

Grünewald, T., and Lehning, M.: Are flat-field snow depth measurements representative? A comparison of selected index sites with areal snow depth measurements at the small catchment scale, Hydrol Processes, 29, 1717-1728, 10.1002/hyp.10295, 2015.

Hantel, M., Maurer, C., and Mayer, D.: The snowline climate of the Alps 1961–2010. Theor Appl Climatol, 110, 517, 10.1007/s00704-012-0688-9, 2012.

Hawkins, E., and Sutton, R.: The Potential to Narrow Uncertainty in Regional Climate Predictions, B Am Meteorol Soc, 90, 1095-+, 10.1175/2009BAMS2607.1, 2009.

Haylock, M.R., Hofstra, N., Klein Tank, A.M.G., Klok, E.J., Jones, P.D., and New, M.: A European daily high-resolution gridded data set of surface temperature and precipitation for 1950–2006, J Geophys Res, 113, D20119, 10.1029/2008JD010201.

Held, I. M., and Soden, B. J.: Robust responses of the hydrological cycle to global warming, J Climate, 19, 5686-5699, 10.1175/Jcli3990.1, 2006.

IPCC: Climate Change 2013: The Physical Science Basis. Contribution of Working Group I to the Fifth Assessment Report of the Intergovernmental Panel on Climate Change, Cambridge University Press, Cambridge, United Kingdom and New York, NY, USA, 1535 pp., 2013.

Isotta, F. A., Frei, C., Weilguni, V., Tadic, M. P., Lassegues, P., Rudolf, B., Pavan, V., Cacciamani, C., Antolini, G., Ratto, S. M., Munari, M., Micheletti, S., Bonati, V., Lussana, C., Ronchi, C., Panettieri, E., Marigo, G., and Vertacnik, G.: The climate of daily precipitation in the Alps: development and analysis of a high-resolution grid dataset from pan-Alpine rain-gauge data, Int J Climatol, 34, 1657-1675, 10.1002/joc.3794, 2014.

Jacob, D., Petersen, J., Eggert, B., Alias, A., Christensen, O. B., Bouwer, L. M., Braun, A., Colette, A., Déqué, M., Georgievski, G., Georgopoulou, E., Gobiet, A., Menut, L., Nikulin, G., Haensler, A., Hempelmann, N., Jones, C., Keuler, K., Kovats, S., Kröner, N., Kotlarski, S., Kriegsmann, A., Martin, E., van Meijgaard, E., Moseley, C., Pfeifer, S., Preuschmann, S., Radermacher, C., Radtke, K., Rechid, D., Rounsevell, M., Samuelsson, P., Somot, S., Soussana, J. F., Teichmann, C., Valentini, R., Vautard, R., Weber, B., and Yiou, P.: EURO-CORDEX: new high-resolution climate change projections for European impact research, Reg Environ Change, 14, 563-578, 10.1007/s10113-013-0499-2, 2014.

Keller, D. E., Fischer, A. M., Liniger, M. A., Appenzeller, C. and Knutti, R.: Testing a weather generator for downscaling climate change projections over Switzerland. Int J Climatol, doi:10.1002/joc.4750, 2016.

Kienzle, S. W.: A new temperature based method to separate rain and snow, Hydrol Process, 22, 5067-5085, 10.1002/hyp.7131, 2008.

Kotlarski, S., Bosshard, T., Lüthi, D., Pall, P., and Schär, C.: Elevation gradients of European climate change in the regional climate model COSMO-CLM. Clim Change, 112, 189-215, 10.1007/s10584-011-0195-5, 2012.

Kotlarski, S., Keuler, K., Christensen, O. B., Colette, A., Deque, M., Gobiet, A., Goergen, K., Jacob, D., Luthi, D., van Meijgaard, E., Nikulin, G., Schar, C., Teichmann, C., Vautard, R., Warrach-Sagi, K., and Wulfmeyer, V.: Regional climate modeling on European scales: a joint standard evaluation of the EURO-CORDEX RCM ensemble, Geosci Model Dev, 7, 1297-1333, 10.5194/gmd-7-1297-2014, 2014.

Kotlarski, S., Lüthi, D., and Schär, C.: The elevation dependency of 21st century European climate change: an RCM ensemble perspective, Int J Climatol, 35, 3902-3920, 10.1002/joc.4254, 2015.

Krasting, J. P., Broccoli, A. J., Dixon, K. W., and Lanzante, J. R.: Future Changes in Northern Hemisphere Snowfall. J Clim, 26, 7813-7828, 10.1175/JCLI-D-12-00832.1, 2013.

Laternser, M., and Schneebeli, M.: Long-term snow climate trends of the Swiss Alps (1931-99), Int J Climatol, 23, 733-750, 10.1002/joc.912, 2003.

Marty, C.: Regime shift of snow days in Switzerland, Geophys Res Lett, 35, 10.1029/2008gl033998, 2008.

Marty, C., and Blanchet, J.: Long-term changes in annual maximum snow depth and snowfall in Switzerland based on extreme value statistics, Clim Change, 111, 705-721, 2011.

McAfee, S. A., Walsh, J., and Rupp, T. S.: Statistically downscaled projections of snow/rain partitioning for Alaska, Hydrol Process, 28, 3930-3946, 10.1002/hyp.9934, 2014.

MeteoSchweiz: Klimareport 2015. Bundesamt für Meteorologie und Klimatologie MeteoSchweiz, Zürich.

MeteoSwiss: Daily Precipitation (final analysis): RhiresD: www.meteoswiss.admin.ch/content/dam/meteoswiss/de/service-und-publikationen/produkt/raeumliche-daten-niederschlag/doc/ProdDoc_RhiresD.pdf, access: 10.01.2017, 2013a.

MeteoSwiss: Daily Mean, Minimum and Maximum Temperature: TabsD, TminD ,TmaxD: www.meteoswiss.admin.ch/content/dam/meteoswiss/de/service-und-publikationen/produkt/raeumliche-daten-temperatur/doc/ProdDoc_TabsD.pdf, access: 10.01.2017, 2013b.

Moss, R. H., Edmonds, J. A., Hibbard, K. A., Manning, M. R., Rose, S. K., van Vuuren, D. P., Carter, T. R., Emori, S., Kainuma, M., Kram, T., Meehl, G. A., Mitchell, J. F. B., Nakicenovic, N., Riahi, K., Smith, S. J., Stouffer, R. J., Thomson, A. M., Weyant, J. P., and Wilbanks, T. J.: The next generation of scenarios for climate change research and assessment, Nature, 463, 747-756, 10.1038/nature08823, 2010.

Neff, E. L.: How Much Rain Does a Rain Gauge Gauge, J Hydrol, 35, 213-220, 10.1016/0022-1694(77)90001-4, 1977.

O'Gorman, P. A.: Contrasting responses of mean and extreme snowfall to climate change, Nature, 512, 416-U401, 10.1038/nature13625, 2014.

Piazza, M., Boé, J., Terray, L., Pagé, C., Sanchez-Gomez, E., and Déqué, M.: Projected 21st century snowfall changes over the French Alps and related uncertainties, Clim Change, 122, 583-594, 10.1007/s10584-013-1017-8, 2014.

Räisänen, J.: Twenty-first century changes in snowfall climate in Northern Europe in ENSEMBLES regional climate models, Clim Dynam, 46, 339-353, 10.1007/s00382-015-2587-0, 2016.

Rajczak, J., Pall, P., and Schär, C.: Projections of extreme precipitation events in regional climate simulations for Europe and the Alpine Region, J Geophys Res-Atmos, 118, 3610-3626, 10.1002/jgrd.50297, 2013.

Rajczak, J., Kotlarski, S., and Schär, C.: Does Quantile Mapping of Simulated Precipitation Correct for Biases in Transition Probabilities and Spell Lengths?, J Climate, 29, 1605-1615, 10.1175/Jcli-D-15-0162.1, 2016.

Rajczak, J. and Schär, C.: Projections of future precipitation extremes over Europe: a multi-model assessment of climate simulations. J Geophys Res Atmos, in press, 2017.

Richards, F. J.: A Flexible Growth Function for Empirical Use, J Exp Bot, 10, 290-300, 10.1093/Jxb/10.2.290, 1959.

Rummukainen, M.: State-of-the-art with regional climate models, Wiley Interdisciplinary Reviews-Climate Change, 1, 82-96, 10.1002/wcc.8, 2010.

Schär, C., Ban, N., Fischer, E. M., Rajczak, J., Schmidli, J., Frei, C., Giorgi, F., Karl, T. R., Kendon, E. J., Tank, A. M. G. K., O'Gorman, P. A., Sillmann, J., Zhang, X. B., and Zwiers, F. W.: Percentile indices for assessing changes in heavy precipitation events, Clim Change, 137, 201-216, 10.1007/s10584-016-1669-2, 2016.

Scherrer, S. C., Appenzeller, C., and Laternser, M.: Trends in Swiss Alpine snow days: The role of local- and large-scale climate variability, Geophys Res Lett, 31, 10.1029/2004gl020255, 2004.

Schmidli, J., Frei, C., and Vidale, P. L.: Downscaling from GCM precipitation: A benchmark for dynamical and statistical downscaling methods, Int J Climatol, 26, 679-689, 10.1002/joc.1287, 2006.

Schmucki, E., Marty, C., Fierz, C., and Lehning, M.: Simulations of 21st century snow response to climate change in Switzerland from a set of RCMs, Int J Climatol, 35, 3262-3273, 10.1002/joc.4205, 2015a.

Schmucki, E., Marty, C., Fierz, C., Weingartner, R. and Lehning, M.: Impact of climate change in Switzerland on socioeconomic snow indices, Theor Appl Climatol, in press, 10.1007/s00704-015-1676-7, 2015b.

Serquet, G., Marty, C., and Rebetez, M.: Monthly trends and the corresponding altitudinal shift in the snowfall/precipitation day ratio, Theor Appl Climatol, 114, 437-444, 10.1007/s00704-013-0847-7, 2013.Sevruk, B.:

Der Niederschlag in der Schweiz, Geographisches Institut der Eidgenössischen Technischen Hochschule in Zürich, Abteilung Hydrologie, Zurich, Switzerland, 1985.

SFOE, Hydropower: http://www.bfe.admin.ch/themen/00490/00491/index.html?lang=en, access: 16.09.2016, 2014.

Smiatek, G., Kunstmann, H., and Senatore, A.: EURO-CORDEX regional climate model analysis for the Greater Alpine Region: Performance and expected future change, J Geophys Res-Atmos, 121, 7710-7728, 10.1002/2015JD024727, 2016.

Soncini, A., and Bocchiola, D.: Assessment of future snowfall regimes within the Italian Alps using general circulation models, Cold Reg Sci Technol, 68, 113-123, 10.1016/j.coldregions.2011.06.011, 2011.

Steger, C., Kotlarski, S., Jonas, T., and Schär, C.: Alpine snow cover in a changing climate: a regional climate model perspective, Clim Dynam, 41, 735-754, 10.1007/s00382-012-1545-3, 2013.

Techel, F., Stucki, T., Margreth, S., Marty, C., and Winkler, K.: Schnee und Lawinen in den Schweizer Alpen. Hydrologisches Jahr 2013/14, WSL-Institut für Schnee- und Lawinenforschung SLF, Birmensdorf, Switzerland, 2015.

Terzago, S., von Hardenberg, J., Palazzi, E., and Provenzale, A.: Snow water equivalent in the Alps as seen by gridded datasets, CMIP5 and CORDEX climate models. The Cryosphere Discussion, 10.5194/tc-2016-280, 2017.

Torma, C., Giorgi, F., and Coppola, E.: Added value of regional climate modeling over areas characterized by complex terrain Precipitation over the Alps, J Geophys Res-Atmos, 120, 3957-3972, 10.1002/2014JD022781, 2015.

Vautard, R., Gobiet, A., Jacob, D., Belda, M., Colette, A., Déqué, M., Fernandez, J., Garcia-Diez, M., Goergen, K., Guttler, I., Halenka, T., Karacostas, T., Katragkou, E., Keuler, K., Kotlarski, S., Mayer, S., van Meijgaard, E., Nikulin, G., Patarcic, M., Scinocca, J., Sobolowski, S., Suklitsch, M., Teichmann, C., Warrach-Sagi, K., Wulfmeyer, V., and Yiou, P.: The simulation of European heat waves from an ensemble of regional climate models within the EURO-CORDEX project, Clim Dynam, 41, 2555-2575, 10.1007/s00382-013-1714-z, 2013.

Weingartner, R., Schädler, B., and Hänggi, P.: Auswirkungen der Klimaänderung auf die schweizerische Wasserkraftnutzung, Geographica Helvetica, 68, 239-248, 2013.

Yang, D. Q., Elomaa, E., Tuominen, A., Aaltonen, A., Goodison, B., Gunther, T., Golubev, V., Sevruk, B., Madsen, H., and Milkovic, J.: Wind-induced precipitation undercatch of the Hellmann gauges, Nord Hydrol, 30, 57-80, 1999.

Zubler, E. M., Scherrer, S. C., Croci-Maspoli, M., Liniger, M. A., and Appenzeller, C.: Key climate indices in Switzerland; expected changes in a future climate, Clim Change, 123, 255-271, 10.1007/s10584-013-1041-8, 2014.

Zubler, E. M., Fischer, A. M., Liniger, M. A., and Schlegel, T.: Auftausalzverbrauch im Klimawandel, MeteoSwiss, Zurich, Switzerland, Fachbericht 253, 2015.

Figures

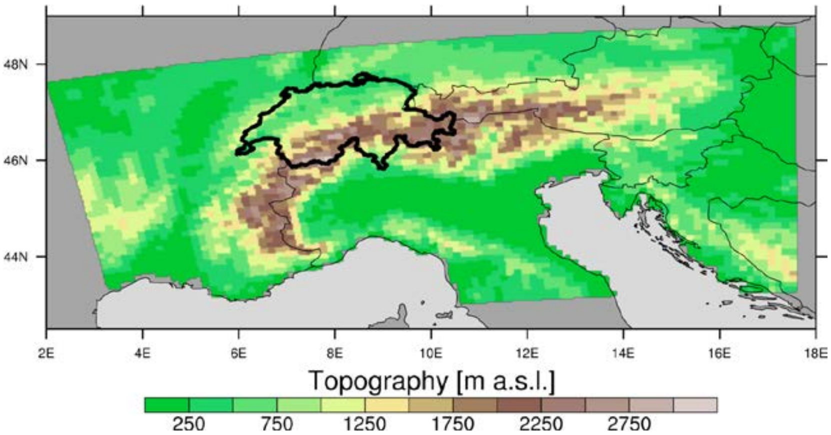

Figure 1 GTOPO30 topography (*https://lta.cr.usgs.gov/GTOPO30*) aggregated to the EUR-11 (0.11°) RCM grid. The coloured area shows the Alpine domain used for the assessment of snowfall projections. The bold black outline marks the Swiss sub-domain used for the assessment of the bias adjustment approach.

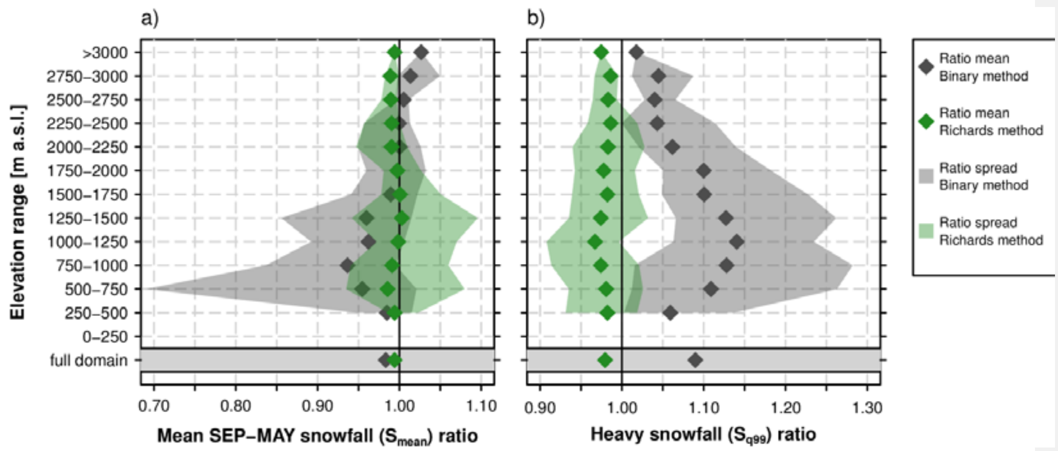

Figure 2 Snowfall ratios for the Binary and Richards snow fractionation method. Ratios represent the quotient of the snowfall as estimated by the respective method and the snowfall as estimated by the *Subgrid* method. Ratios are valid at the coarse-resolution grid (12 km). a) Ratios for mean snowfall, S_{mean}. b) Ratios for heavy snowfall, S_{q99}. Ratio means were derived after averaging the corresponding snowfall index for 250 m elevation intervals in Switzerland while the ratio spread represents the minimum and maximum grid point-based ratios in the corresponding elevation interval. This analysis is entirely based on the observational data sets TabsD and RhiresD.

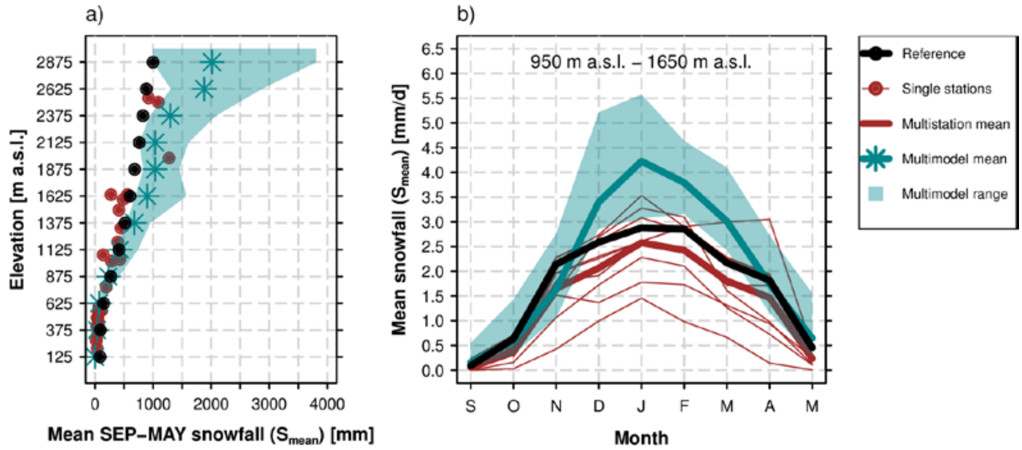

Figure 3 Comparison of measured fresh snow sums of 29 MeteoSwiss stations (red) against simulated RCM raw snowfall in Switzerland (green) and against the 2 km reference snowfall grid obtained by employing the *Subgrid method* (black) in the EVAL period 1971-2005. a) Mean September – May snowfall vs. elevation. Both the simulation data (green) and the reference data (black) are based on the spatio-temporal mean of 250 m elevation ranges and plotted at the mean elevation of the corresponding interval. b) Seasonal September-May snowfall cycle for the elevation interval 950 m a.s.l. to 1650 m a.s.l.. Simulated multi-model means and spreads are based on a subset of seven EURO-CORDEX simulations of the reduced model set providing raw snowfall as output variable (see Tab. 1).

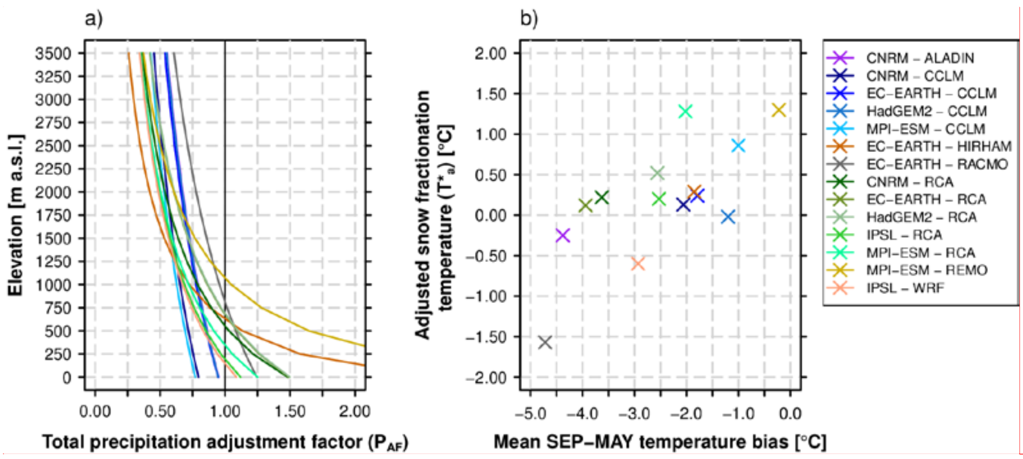

Figure 4 Overview of bias adjustment. a) Elevation-dependent total precipitation adjustment factors, P_{AF}, for the full model set (14~~2~~ GCM-RCM chains; ~~(~~see Eq. 10). b) Scatterplot of mean September to May temperature biases (RCM simulation minus observational analysis) vs. adjusted snow fractionation temperatures, T^*_a.

Comment [Sven1]: As requested, figure has been replaced and now shows the full model set.

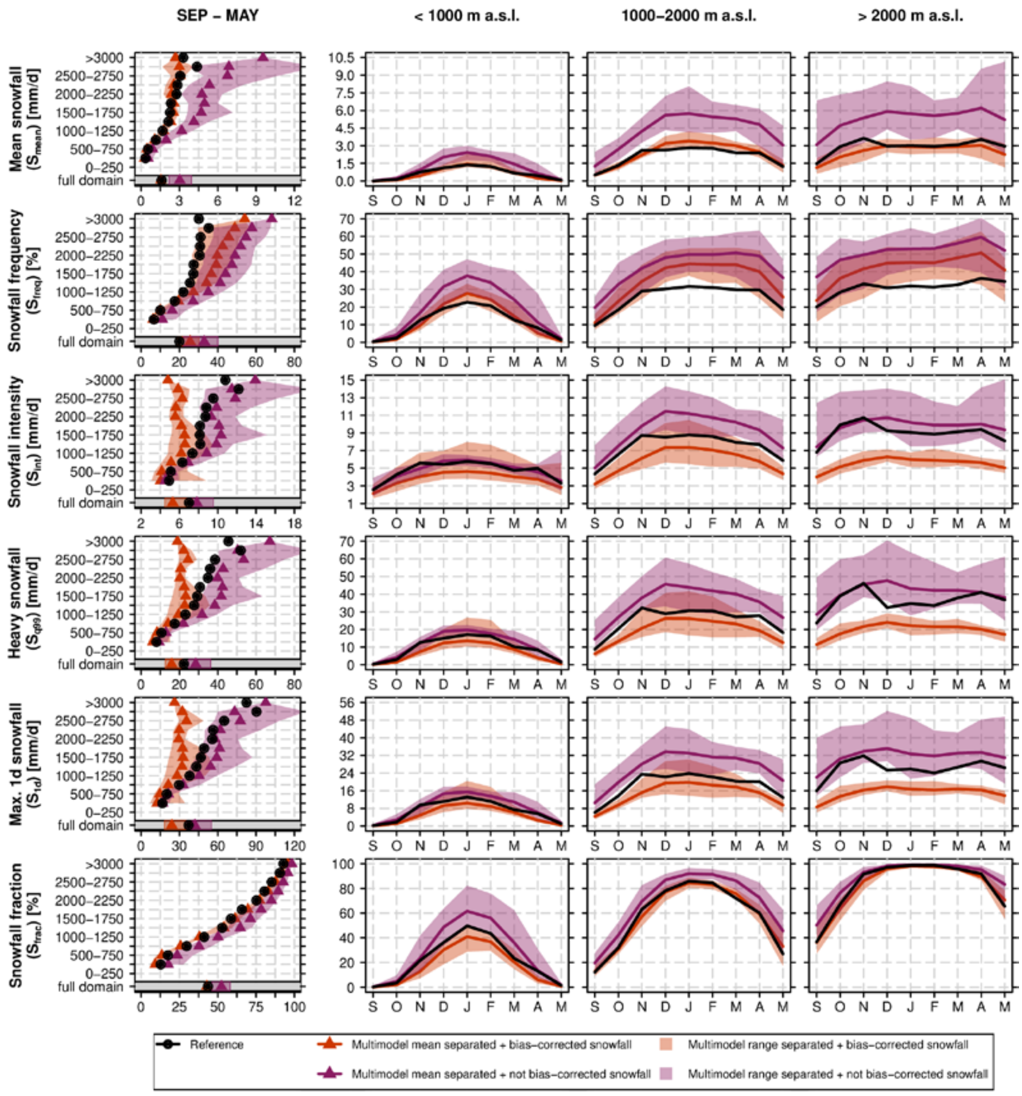

Figure 5 Evaluation of snowfall indices in the EVAL period 1971-2005 for the 12 snowfall separated + bias-adjusted (RCM_{sep+ba}) and 12 snowfall separated + not bias-adjusted ($RCM_{sep+nba}$) RCM simulations of the reduced model set vs. observation-based reference. The first column shows the mean September-May snowfall index statistics vs. elevation while the monthly snowfall indices (spatially averaged over the elevation intervals <1000 m.a.s.l., 1000 m a.s.l.-2000 m a.s.l. and >2000 m a.s.l.) are displayed in columns 2-4.

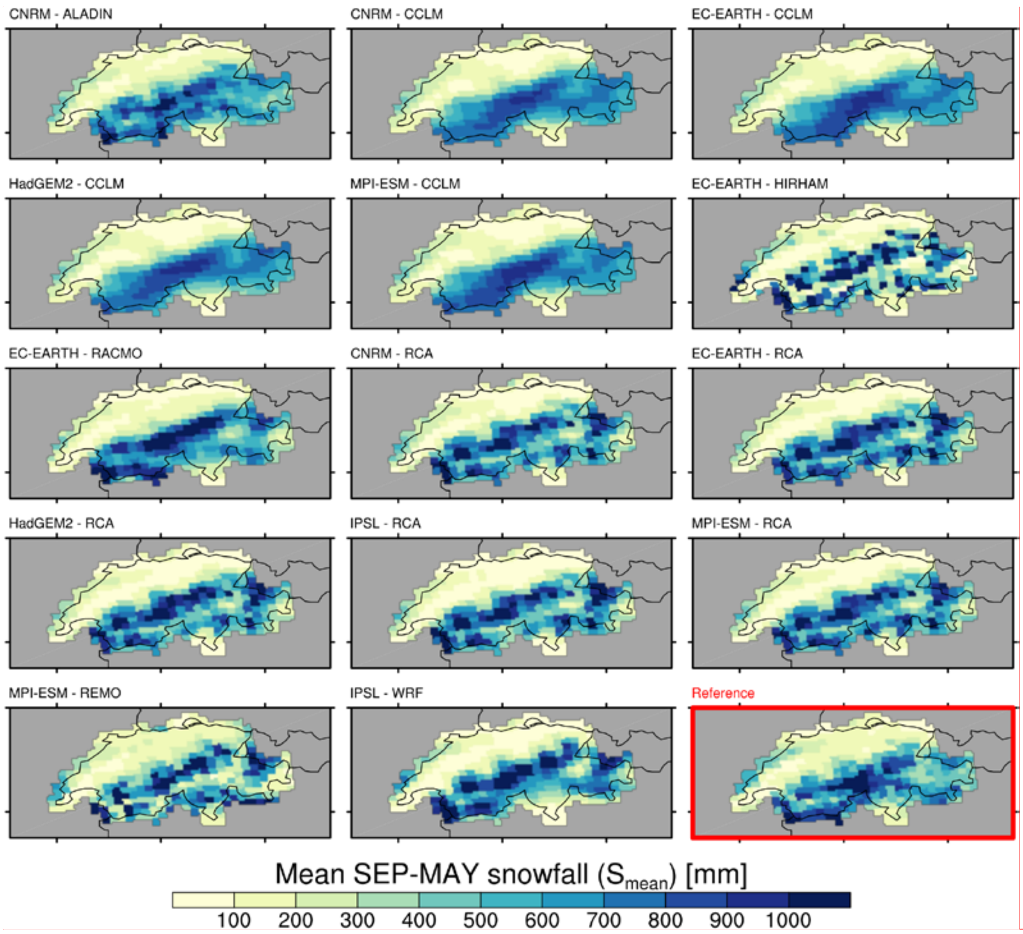

Figure 6 Spatial distribution of mean September-May snowfall, S_{mean}, in the EVAL period 1971-2005 and for the 14~~2~~ snowfall separated + bias-adjusted RCM simulations (RCM_{sep+ba}) of the full model set. ~~Bottom~~ Lower right panel: observation-based reference.

Comment [Sven2]: As requested, figure has been replaced and now shows the full model set.

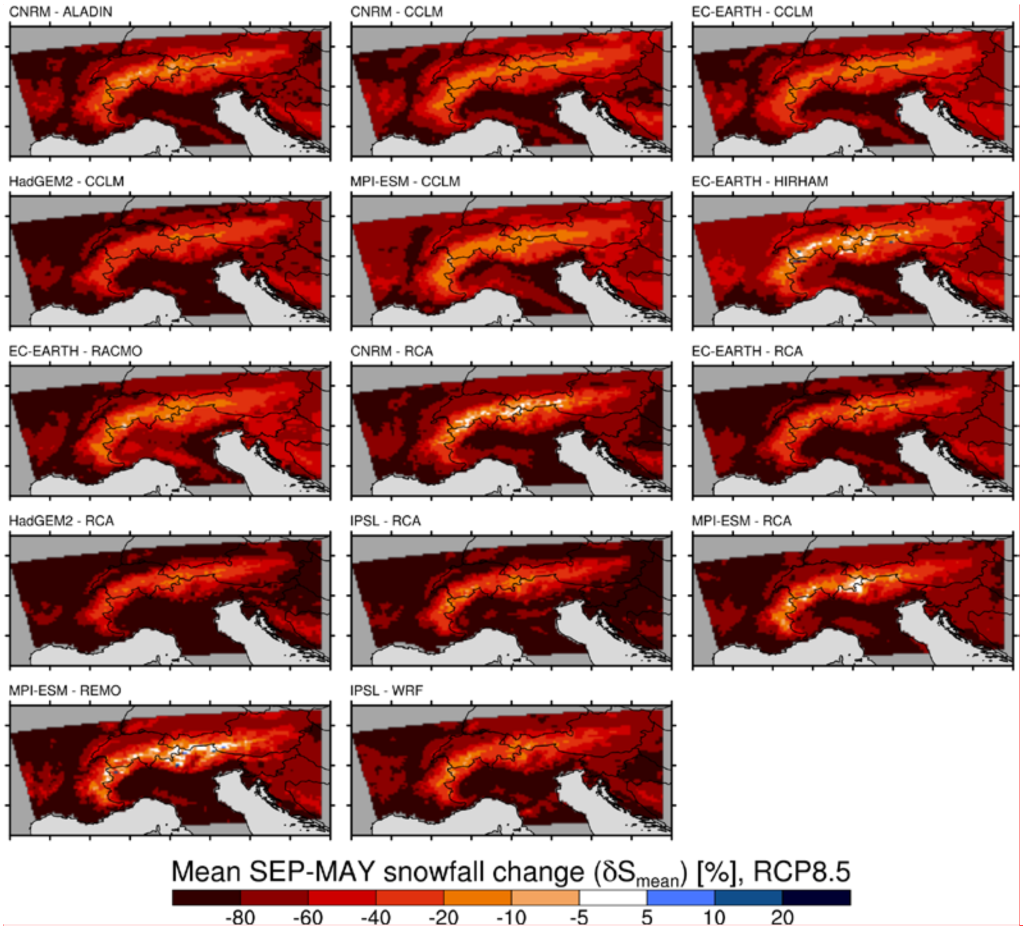

Figure 7 Spatial distribution of relative changes (SCEN period 2070-2099 with respect to CTRL period 1981-2010) in mean September-May snowfall, δS_{mean}, for RCP8.5 and for the ~~12~~ 14 snowfall separated + bias-adjusted RCM simulations (RCM_{sep+ba}) of the full model set. For RCP4.5, see Fig. S~~7~~6.

Comment [Sven3]: As requested, figure has been replaced and now shows the full model set.

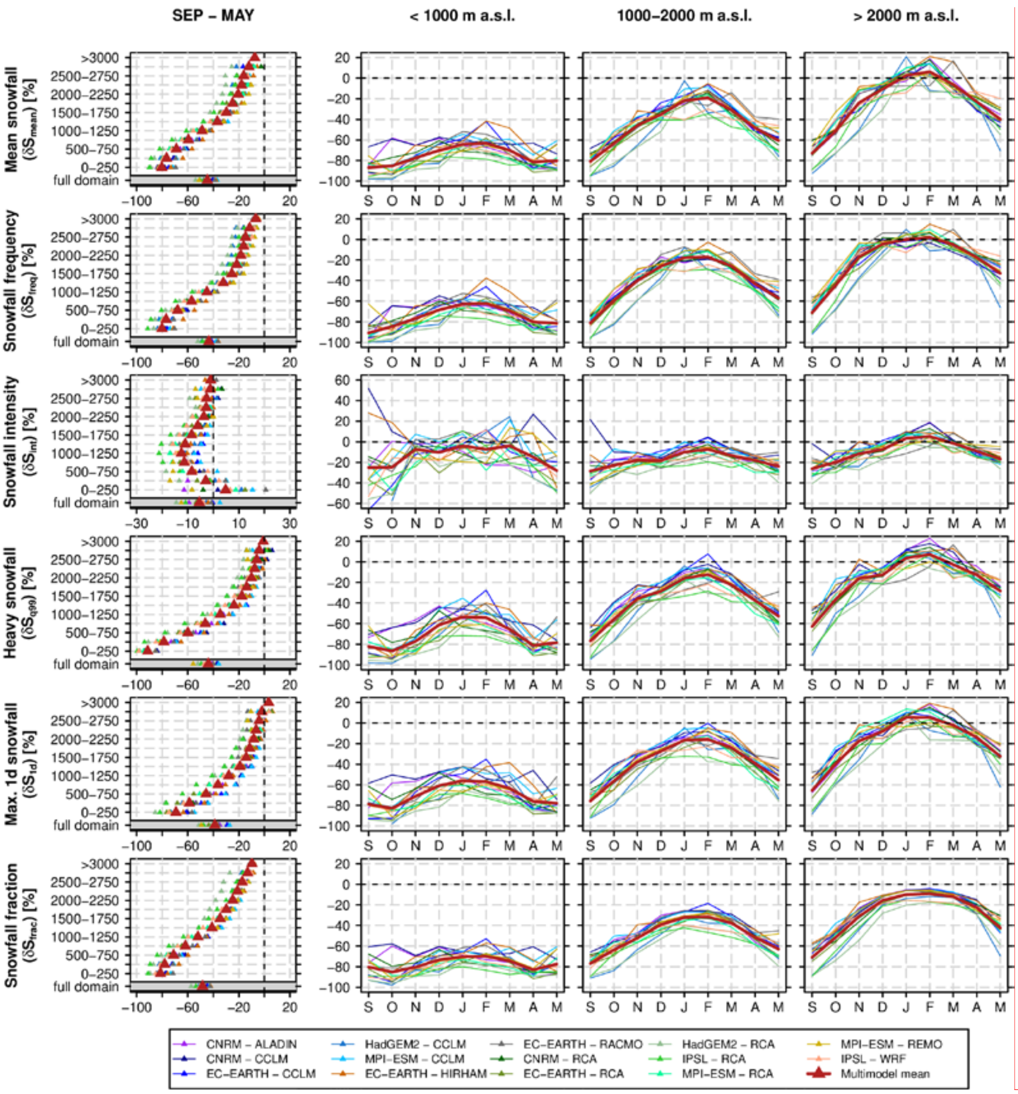

Figure 8 Relative changes (SCEN period 2070-2099 with respect to CTRL period 1981-2010) of snowfall indices based on the 14~~12~~ snowfall separated + bias-adjusted RCM simulations (RCM_{sep+ba}) of the full model set for RCP8.5. The first column shows the mean September-May snowfall index statistics vs. elevation. ~~while m~~Monthly snowfall index changes (spatially averaged over the elevation intervals <1000 m.a.s.l., 1000 m a.s.l.-2000 m a.s.l. and >2000 m a.s.l.) are displayed in columns 2-4.

Comment [Sven4]: As requested, figure has been replaced and now shows the full model set.

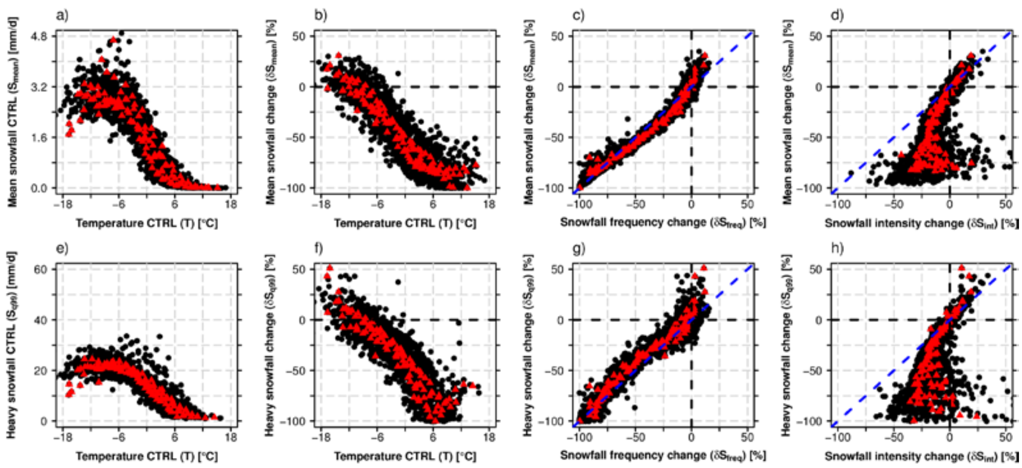

Figure 9 Intercomparison of various snowfall indices and relationship with monthly mean temperature in CTRL. For each panel, the monthly mean statistics for each~~-~~ 250 m elevation interval and for each of the 12 snowfall separated + bias-adjusted (RCMsep+ba) RCM simulations ~~12 individual GCM-RCM chains~~ of the reduced model set (RCM_{sep+ba}) were derived (black circles). Red triangles denote the multi-model mean for a specific month and elevation interval. The monthly statistics were calculated by considering all grid points of the specific elevation intervals which are available for both variables in the corresponding scatterplot only (area consistency). ~~The data were taken from the 12 snowfall separated + bias-adjusted (RCM_{sep+ba}) RCM simulations.~~ Relative changes are based on the RCP8.5 driven simulations (SCEN 2070-2099 wrt. CTRL 1981-2010).

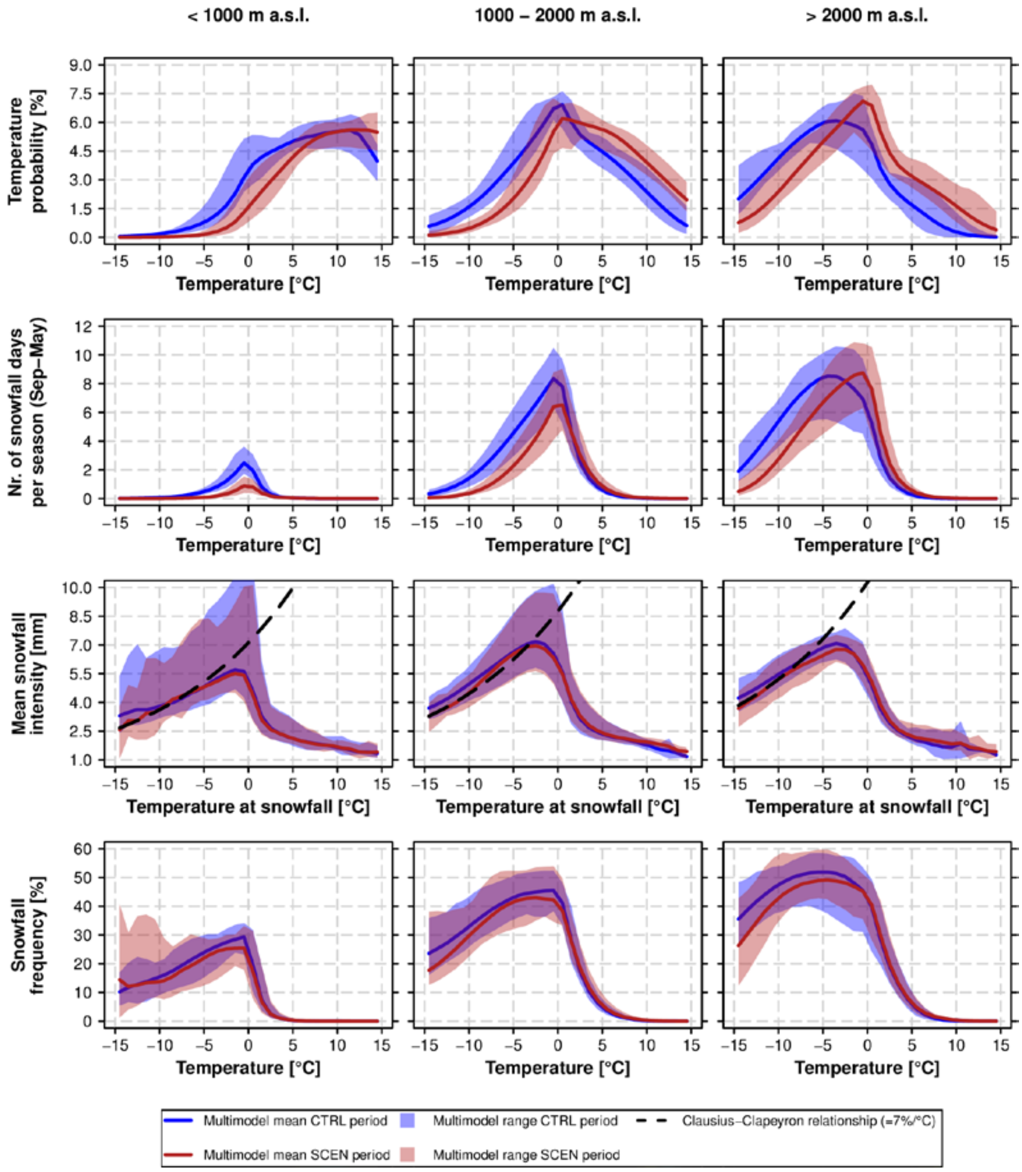

Figure 10 Comparison of temperature probability, snowfall probability and mean snowfall intensity for the CTRL period 1981-2010 and SCEN period 2070-2099 for RCP8.5. The analysis is based on data from the 12 snowfall separated + bias-adjusted RCM simulations (RCM_{sep+ba}) of the reduced model set. The top row depicts the PDF of the daily temperature distribution, while the second row shows the mean number of snowfall days between September and May, i.e., days with S > 1 mm (see Tab. 2), in a particular temperature interval. The third row represents the mean snowfall intensity, S_{int}, for a given snowfall temperature interval. In addition the Clausius-Clapeyron relationship, centred at the -10°C mean S_{int} for SCEN, is displayed by the black dashed line. PDFs and mean S_{int} were calculated by creating daily mean temperature bins of width 1 °C.

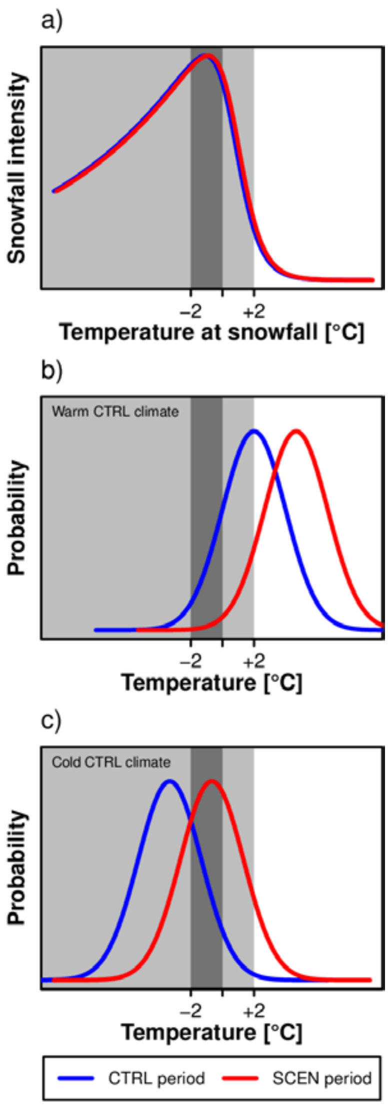

Figure 11 Schematic illustration of the control of changes in snowfall intensity on changes in mean and extreme snowfall. a) Relation between temperature and mean snowfall intensity. b) Daily temperature PDF for a warm control climate (low elevations or transition seasons, i.e., beginning or end of winter). c) Daily temperature PDF for a cold control climate (high elevations or mid-winter). The blue line denotes the historical CTRL period, the red line the future SCEN period. The light grey shaded area represents the overall temperature interval at which snowfall occurs, the dark grey shading shows the preferred temperature interval for heavy snowfall to occur.

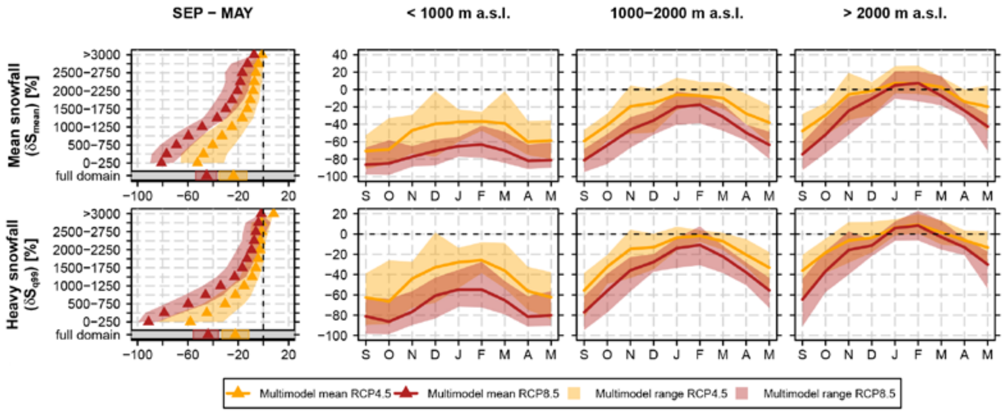

Figure 12 Similar as Figure 8 but showing projected changes of mean snowfall, δS_{mean}, and heavy snowfall, δS_{q99}, for the emission scenarios RCP4.5 and 8.5 and based ~~.~~on the reduced model set. See Fig. S10 for the emission scenario uncertainty of the remaining four snowfall indices. See Fig. S15 for the respective figure based on the full model set.

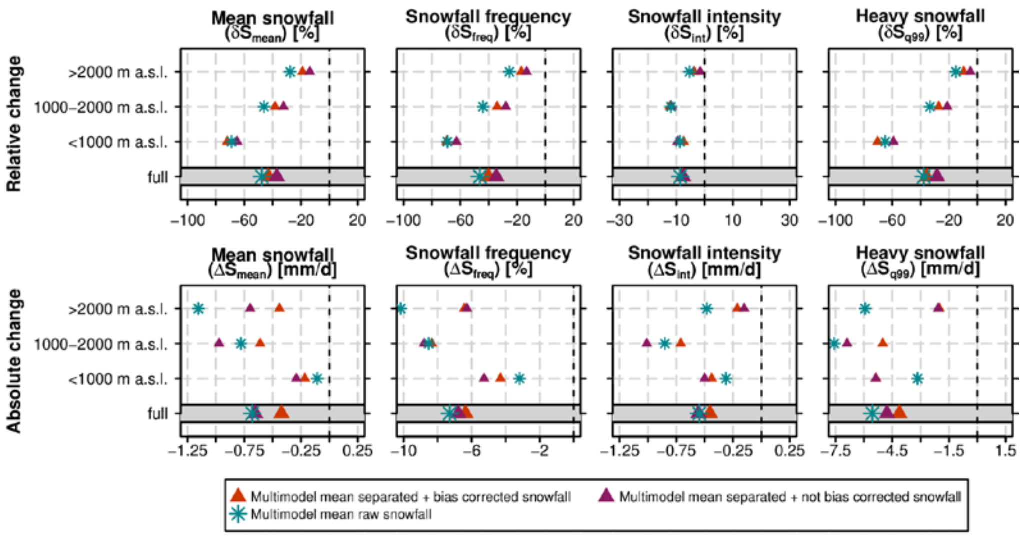

Figure 13 Relative and absolute changes (SCEN period 2070-2099 with respect to CTRL period 1981-2010) of mean September-May snowfall indices based on a subset of seven snowfall separated + bias-adjusted (RCM_{sep+ba}), seven snowfall separated + not bias-adjusted ($RCM_{sep+nba}$) and seven raw snowfall RCM simulations (RCM_{raw}) for RCP8.5. Only RCM simulations of the reduced model set providing raw snowfall as output variable (see Tab. 1) were used in this analysis.

Tables

Table 1 Overview on the ~~12~~ full and the reduced EURO-CORDEX simulations employed in ~~available for~~ this study. ~~The whole model set consists of five RCMs driven by five different GCMs.~~ All experiments were realized on a grid covering the European domain~~,~~ with a horizontal resolution of approximately 12 km (EUR-11) and were run for the emission scenarios RCP4.5 and RCP8.5~~.~~. A subset of ~~seven~~ nine simulations provides raw snowfall, i.e., snowfall flux in kg/m^{2}s, as output variable. The reduced model set excludes experiments that are subject to serious shortcomings (see Supplementary Material, Part B). For full institutional names the reader is referred to the official EURO-CORDEX website www.euro-cordex.net. Note that the EC-EARTH-driven experiments partly employ different realis~~z~~ations of the GCM run, i.e., explicitly sample the influence of internal climate variability in addition to model uncertainty.

RCM	GCM	Acronym	Institute ID	Raw snowfall output	Part of reduced model set
ALADIN53	CNRM-CERFACS-CNRM-CM5	CNRM - ALADIN	CNRM	no	X
CCLM4-8-17	CNRM-CERFACS-CNRM-CM5	CNRM - CCLM	CLMcom/BTU	no	X
CCLM4-8-17	ICHEC-EC-EARTH****	EC-EARTH - CCLM	CLMcom/BTU	no	X
CCLM4-8-17	MOHC-HadGEM2-ES	HadGEM2 - CCLM	CLMcom/ETH	no	X
CCLM4-8-17	MPI-M-MPI-ESM-LR	MPI-ESM - CCLM	CLMcom/BTU	no	X
HIRHAM5	ICHEC-EC-EARTH***	EC-EARTH – HIRHAM	DMI	yes	X
RCA4	CNRM-CERFACS-CNRM-CM5	CNRM - RCA	SMHI	yes	X
RCA4	ICHEC-EC-EARTH****	EC-EARTH - RCA	SMHI	yes	X
RCA4	MOHC-HadGEM2-ES	HadGEM2 - RCA	SMHI	yes	X
RCA4	IPSL-IPSL-CM5A-MR	IPSL - RCA	SMHI	yes	X
RCA4	MPI-M-MPI-ESM-LR	MPI-ESM – RCA	SMHI	yes	X
REMO2009	MPI-M-MPI-ESM-LR*	MPI-ESM – REMO	MPI-CSC	yes	X
RACMO22E	ICHEC-EC-EARTH**	EC-EARTH-RACMO	KNMI	yes	-
WRF331F	IPSL-IPSL-CM5A-MR	IPSL - WRF	IPSL-INERIS	yes	-

* r1i1p1 realisation

** r1i1p1 realisation

*** r3i1p1 realisation

**** r12i1p1 realisation

Table 2 Analysed snowfall indices. The last column indicates the threshold value in the CTRL period for considering a grid cell in the climate changes analysis (grid cells with smaller values are skipped for the respective analysis); first number: threshold for monthly analyses, second number: threshold for seasonal analysis.

Index name	**Acronym**	**Unit**	**Definition**	**Threshold for monthly / seasonal analysis**
Mean snowfall	S_{mean}	mm	(Spatio-)temporal mean snowfall in mm snow water equivalent (only “mm" thereafter).	1 mm / 10 mm
Heavy snowfall	S_{q99}	mm/d	Grid point-based 99% all day snowfall percentile.	1 mm / 1 mm
Max. 1 day snowfall	S_{1d}	mm/d	Mean of each season’s or month’s maximum 1 day snowfall.	1 mm / 1 mm
Snowfall frequency	S_{freq}	%	Percentage of days with snowfall S>1mm/d within a specific time period.	1 % / 1 %
Snowfall intensity	S_{int}	mm/d	Mean snowfall intensity at days with snowfall S>1mm/d within a specific time period.	S_{freq} threshold passed
Snowfall fraction	S_{frac}	%	Percentage of total snowfall, S_{tot}, on total precipitation, P_{tot}, within a specific time period.	1 % / 1 %

Future snowfall in the Alps: Projections based on the EURO-CORDEX regional climate models

Prisco Frei [1], Sven Kotlarski [2,*], Mark A. Liniger [2], Christoph Schär [1]

[1] Institute for Atmospheric and Climate Sciences, ETH Zurich, CH-8006, Zurich, Switzerland
[2] Federal Office of Meteorology and Climatology, MeteoSwiss, CH-8058 Zurich-Airport, Switzerland

[*] Corresponding author: *sven.kotlarski@meteoswiss.ch*

~~–~~Supplementary Material, Part A General Analysis~~–~~

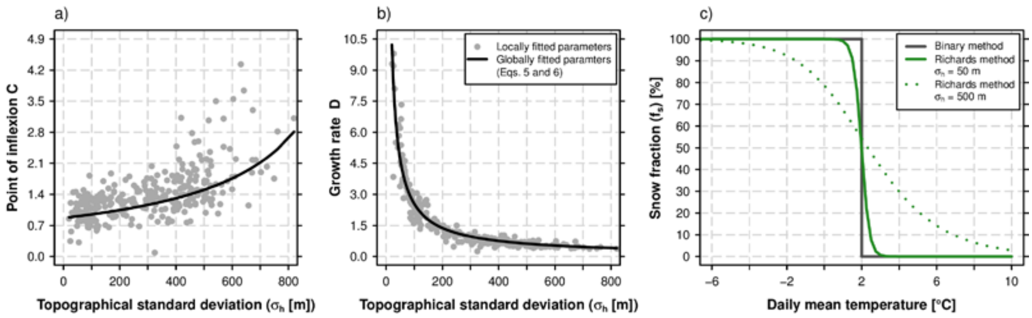

Figure S1 a) and b) Expressing the point of inflexion C and the growth rate D of the Richards equation as a function of the subgrid topographical standard deviation. Grey circles: Fitted parameters for each grid cell in the Swiss domain. Black line: Global fit. c) Example for deriving the daily snow fraction *sf* based on the binary method with a snow fractionation temperature T^*=2°C (gray line) and based on the Richards method assuming subgrid topographical standard deviations of 50 m (solid green line) and 500 m (dotted green line).

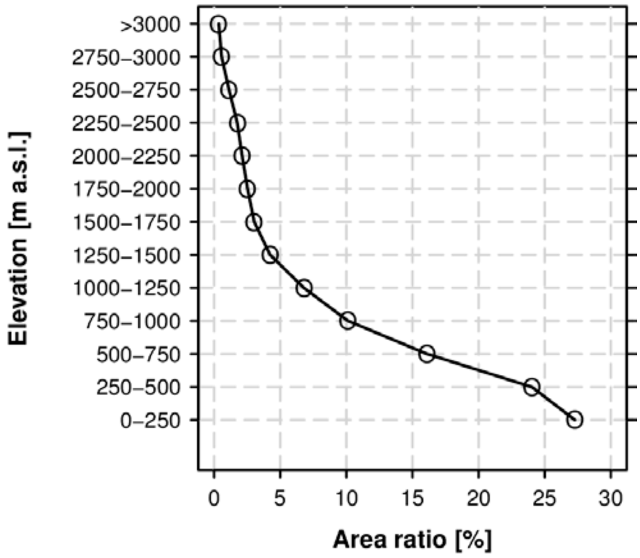

Figure S2 Elevation-area distribution of the Alpine analysis domain (see Fig. 1 of the main manuscript) based on the high-resolution GTOPO30 digital elevation model (https://lta.cr.usgs.gov/GTOPO30) aggregated to a regular grid of 1.25 arc seconds (about 2 km). The area ratio provides the percentage contribution of a given elevation interval to the total area assuming equal grid cell areas.

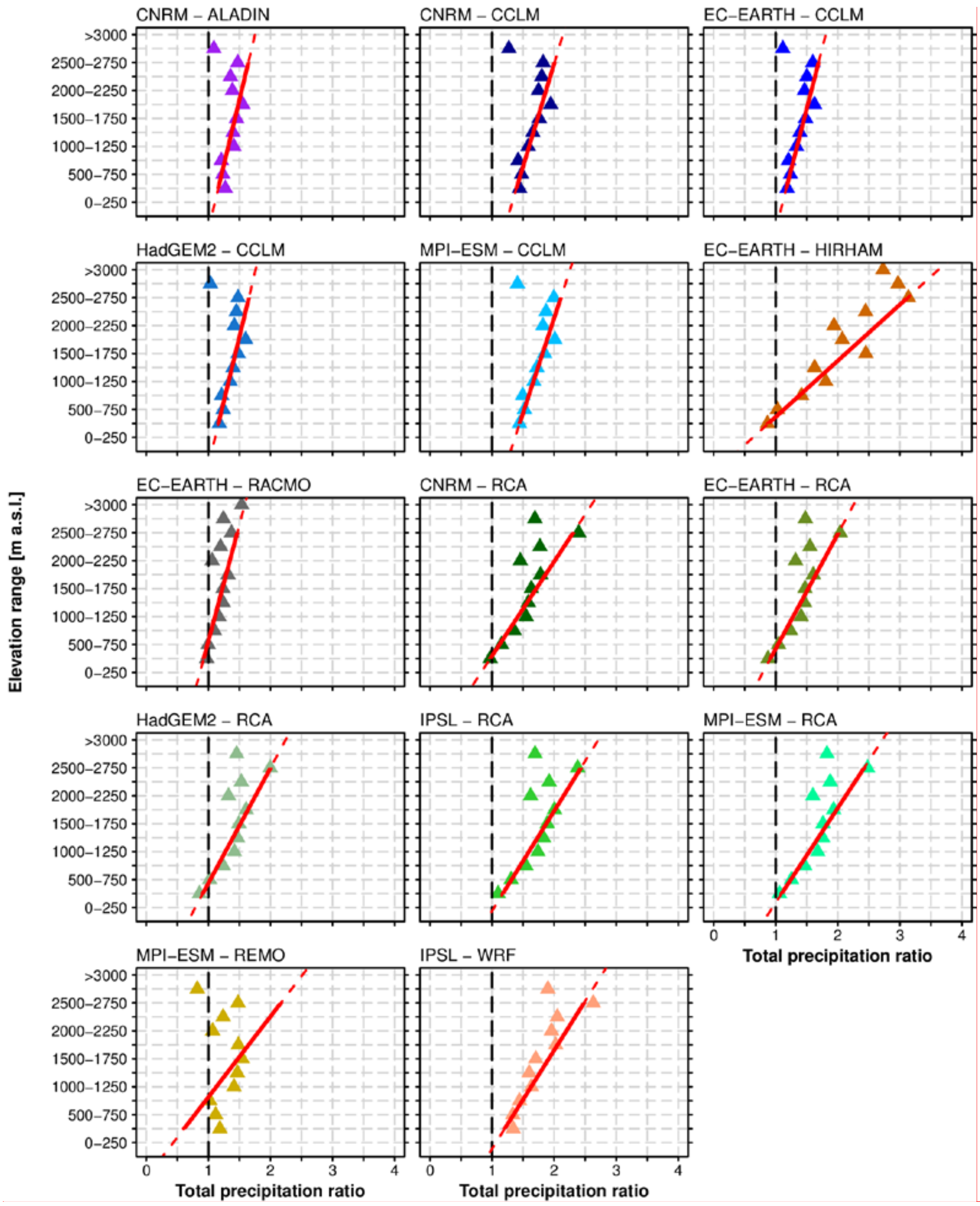

Figure S3: Ratios (RCM simulations of the full model set divided by observational analysis) of total precipitation sums from September to May in 1971 - 2005 vs. elevation for the Swiss domain. The linear regression line, applied to the ratios for elevations between 250 m a.s.l. and 2750 m a.s.l., is represented by the red line.

Comment [Sven5]: Figure has been replaced and now shows the full model set.

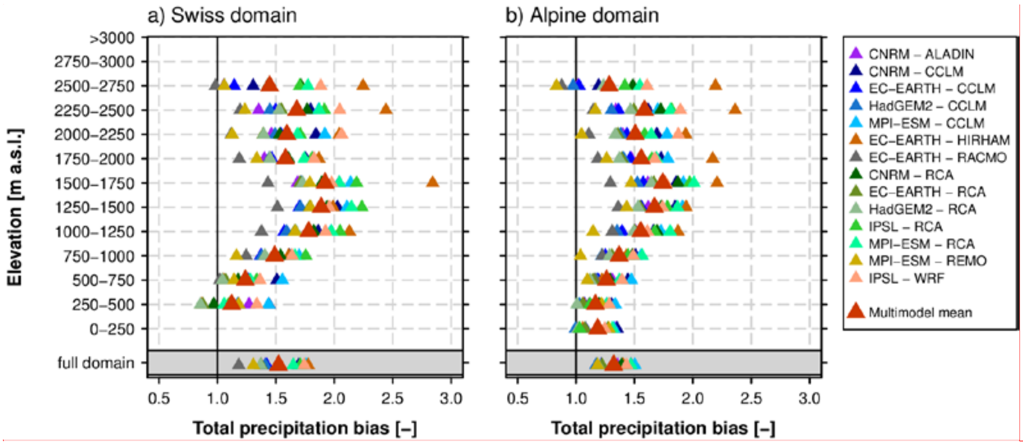

Figure S4: Total winter (SEP-MAY) precipitation bias (expressed as quotient between RCM simulations of the full model set and observations) in the EVAL period 1971-2005 for individual elevation intervals and for the full domain (lowermost row). Left panel: Swiss domain only. Right panel: Entire Alpine analysis domain (cf. Fig. 1). Observational reference: EOBS version 13.1 (Haylock et al., 2008) on 0.22° interpolated to the 0.11° RCM grid by nearest neighbour interpolation.

Comment [Sven6]: Figure has been replaced and now shows the full model set.

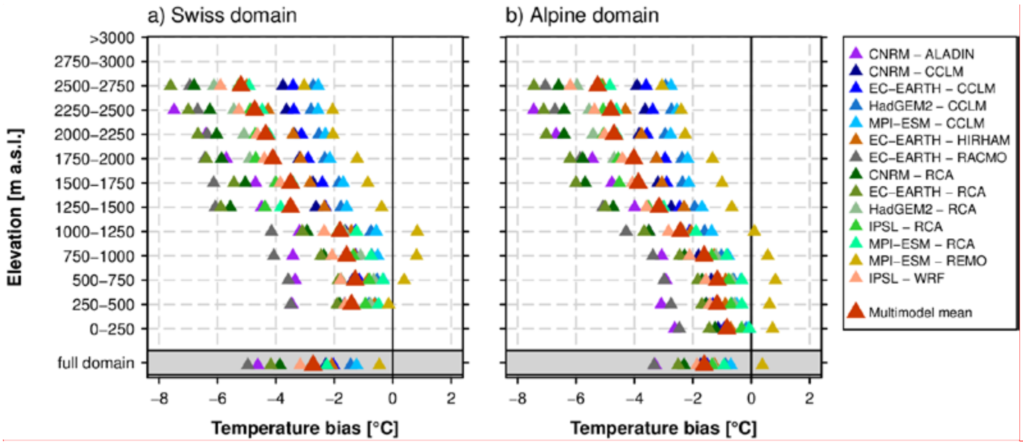

Figure S5: As Figure S4 but for the winter (SEP-MAY) temperature bias.

Comment [Sven7]: Figure has been replaced and now shows the full model set.

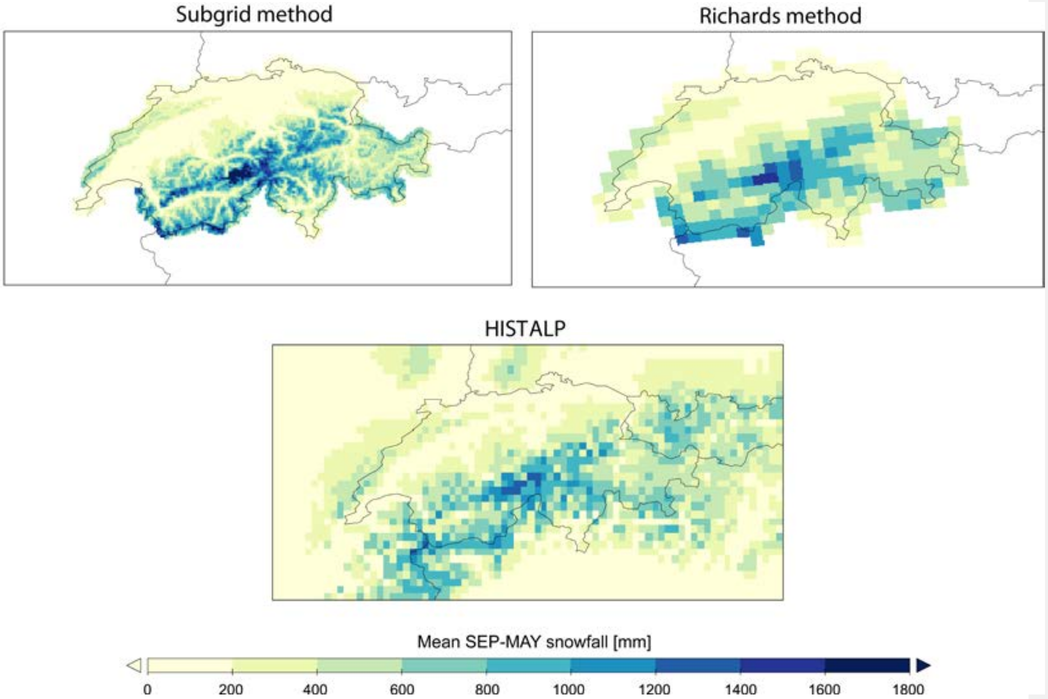

Figure S6 Mean September-May snowfall sum [mm] in the period 1971-2005 as represented by the 2 km snowfall reference (*Subgrid method*; upper left), the 12 km snowfall reference on the RCM grid (*Richards method*; upper right) and the HISTALP dataset (Chimani et al., 2011; lower).

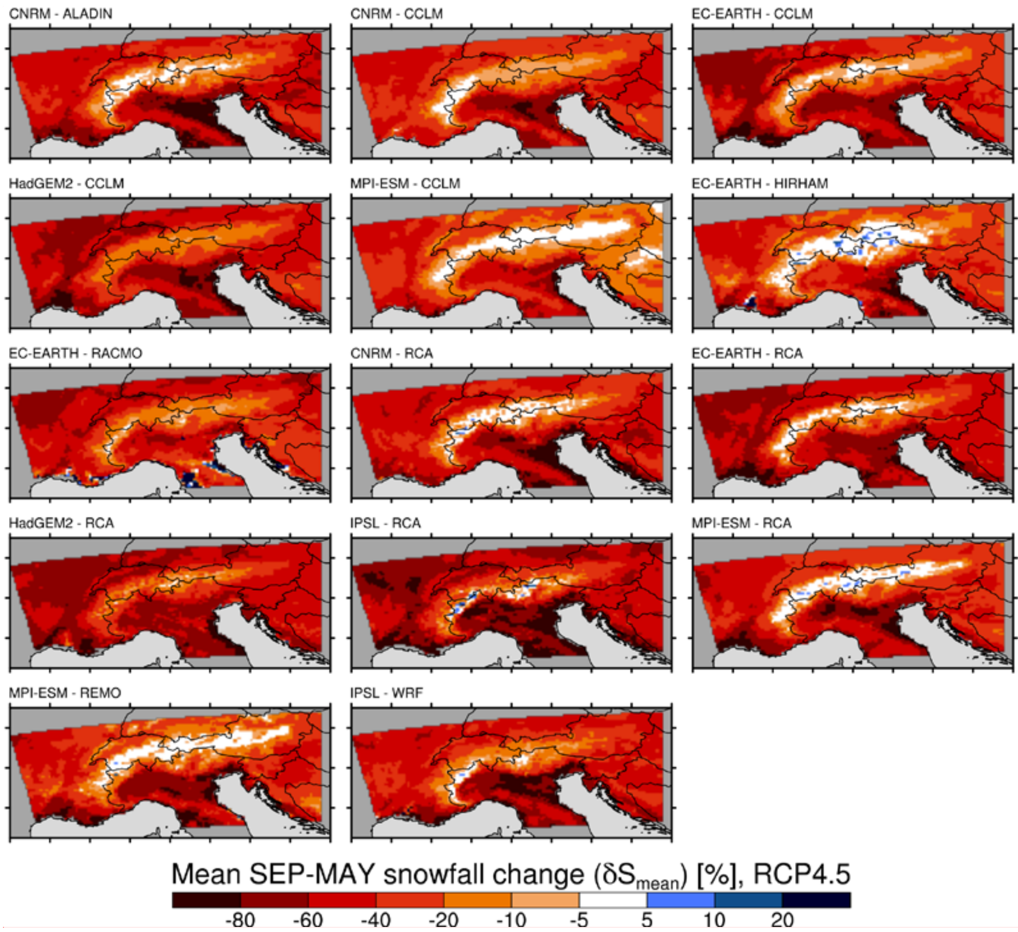

Figure S7 Spatial distribution of relative changes (SCEN period 2070-2099 with respect to CTRL period 1981-2010) in mean September-May snowfall, δS_{mean}, for RCP4.5 and for the 14~~12~~ snowfall separated + bias-adjusted RCM simulations (RCM_{sep+ba}) of the full model set.

Comment [Sven8]: Figure has been replaced and now shows the full model set.

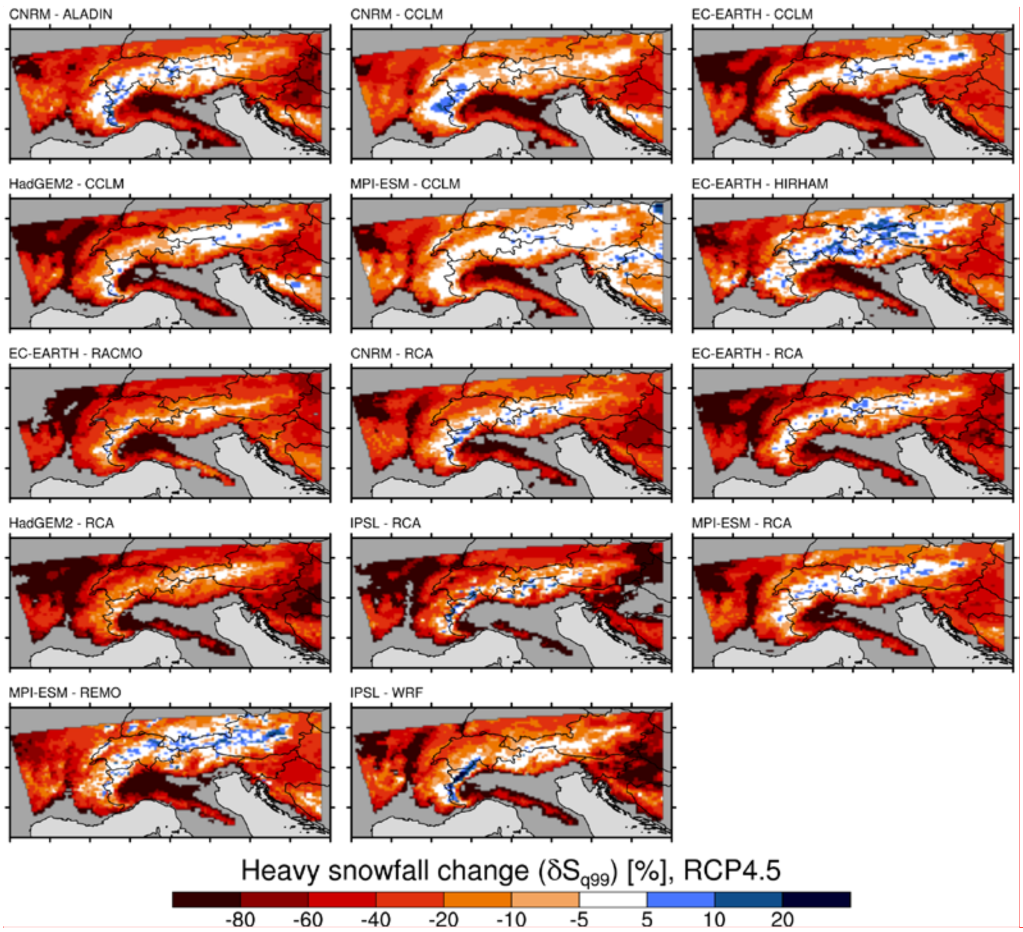

Figure S8 Spatial distribution of relative changes (SCEN period 2070-2099 with respect to CTRL period 1981-2010) in heavy snowfall, δS_{q99}, for RCP4.5 and for the 14~~12~~ snowfall separated + bias-adjusted RCM simulations (RCM_{sep+ba}) of the full model set.

Comment [Sven9]: Figure has been replaced and now shows the full model set.

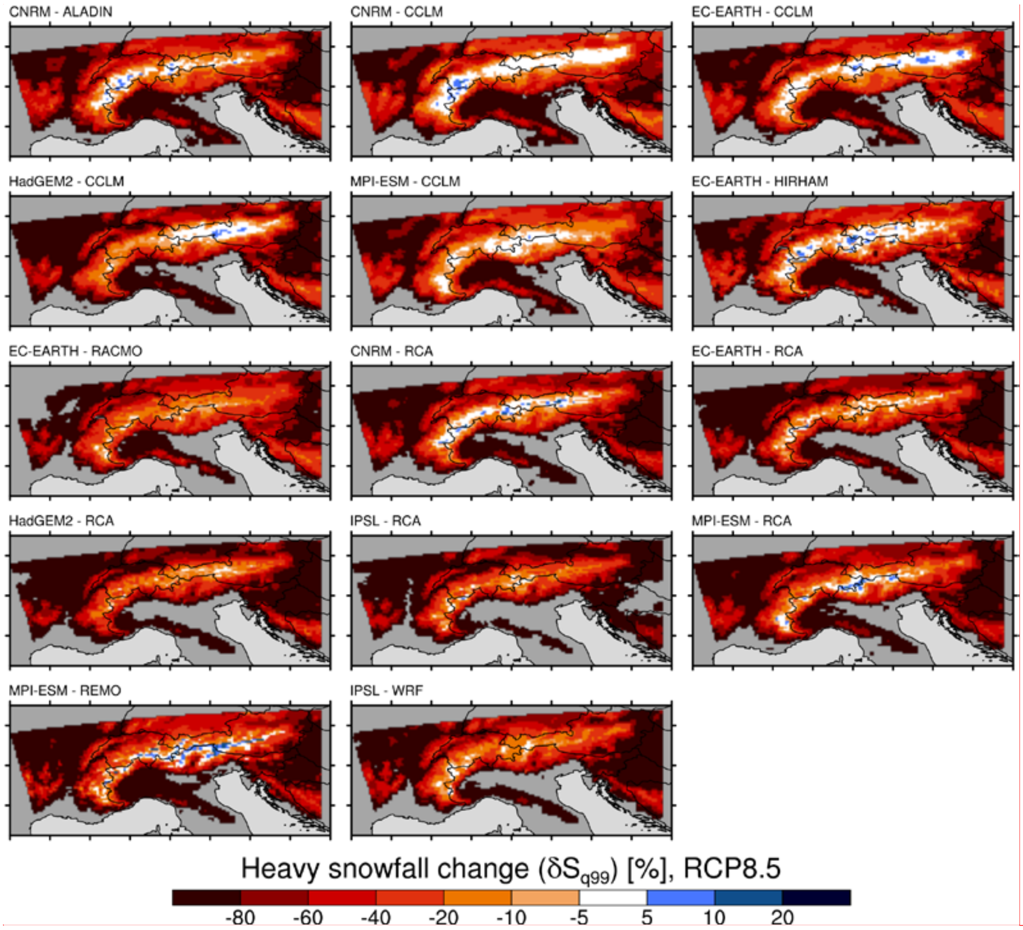

Figure S9 Spatial distribution of relative changes (SCEN period 2070-2099 with respect to CTRL period 1981-2010) in heavy snowfall, δS_{q99}, for RCP8.5 and for the 14~~12~~ snowfall separated + bias-adjusted RCM simulations (RCM_{sep+ba}) of the full model set.

Comment [Sven10]: Figure has been replaced and now shows the full model set.

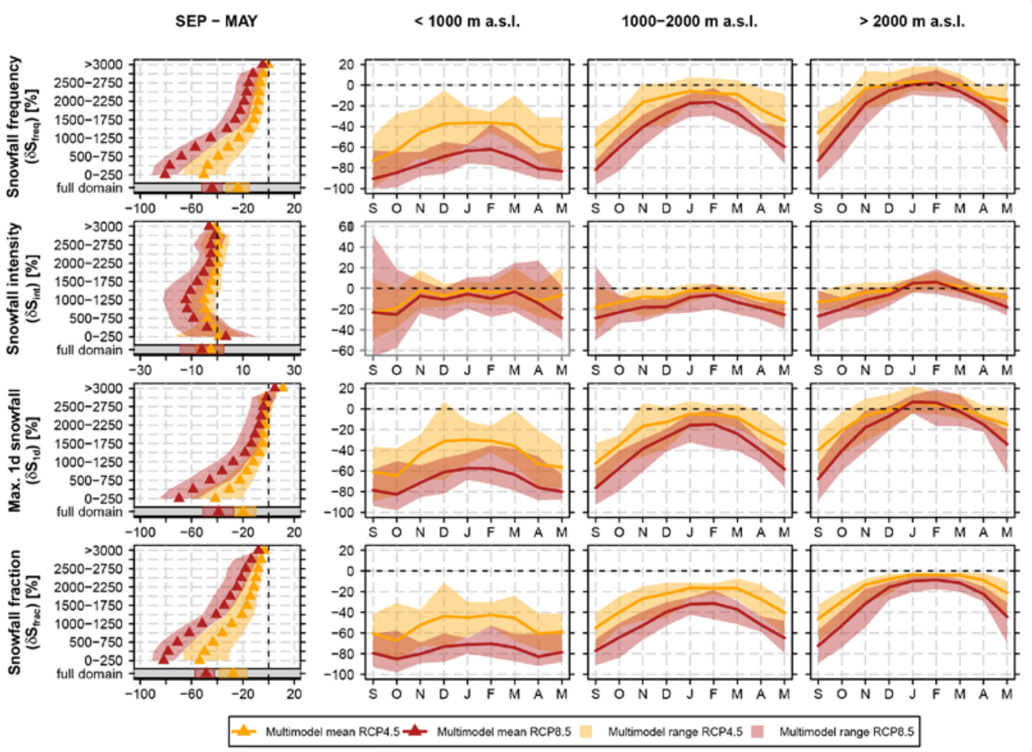

Figure S10 Relative changes (SCEN period 2070-2099 with respect to CTRL period 1981-2010) of max. 1 day snowfall, δS_{1d}, snowfall frequency, δS_{freq}, snowfall intensity, δS_{freq}, and snowfall fraction, δS_{frac}, based on the 12 snowfall separated + bias-adjusted (RCM_{sep+ba}) RCM simulations <u>of the reduced model set</u> for RCP4.5 and RCP8.5, each. The first column shows the mean September-May snowfall index statistics vs. elevation while monthly snowfall index changes (spatially averaged over the elevation intervals <1000 m.a.s.l., 1000 m a.s.l.-2000 m a.s.l. and >2000 m a.s.l.) are displayed in columns 2-4.

Supplementary Material, Part B

Climate Model Selection

Our analysis initially considered all EURO-CORDEX GCM-RCM combinations available in December 2016 that provide experiments for the higher EUR-11 resolution and for both RCP4.5 and RCP8.5. Out of this initial set individual combinations were either completely or partly removed from the analysis due to the reasons outlined below. The reduced model set consists of 12 GCM-RCM chains (see Table 1 of the main manuscript) and is consistent with the current model selection for the upcoming CH2018 Swiss Climate Scenarios (*www.ch2018.ch*). In the present work all ensemble-based analyses that do not allow an identification of individual experiments are carried out for this reduced set only. Fig. 12 of the main manuscript, however, is replicated for the full set which allows an intercomparison of the results for both selections (Fig. S15).

MPI-ESM-REMO

Two realisations of the GCM-RCM chain MPI-ESM-REMO are available (initial condition ensemble sampling internal climate variability). In order to avoid mixing GCM-RCM sampling with pure internal climate variability sampling, the second realisation of this model chain was removed and only the first one was considered.

HadGEM2-RACMO and EC-EARTH-RACMO

These two model chains are subject to a widespread continuous accumulation of snow cover at high alpine grid cells in the course of the 21st century. For individual grid cells several tens of meters of snow water equivalent are obtained. The extensive snow accumulation has obvious feedbacks on the climate change signal of 2m temperature: Temperature change signals are considerably lower at the affected grid cells than in surrounding regions. The summer season JJA, which is excluded from our analysis, is most affected (Fig. S11). But also neighbouring months are concerned (Fig. S12). The ultimate reason for this behaviour is not clear, but the issue is potentially critical for our analysis as 2m temperature change signals directly influence future snowfall changes via changes of the precipitation phase. HadGEM2-RACMO, which is subject to the highest spatial variability of temperature change signals in the May/September mean, has therefore been completely omitted in this study. EC-EARTH-RACMO is considered in the full but not in the reduced model set (see Table 1 of the main manuscript).

IPSL-WRF

This model chain is subject to suspicious precipitation and temperature change signals in the northern part of the Alps that at least partly have to be considered to be unphysical. The most affected season is summer (JJA), but also adjacent months are concerned. In detail, the RCM output in terms of precipitation along the northern flanks of the Alps shows a very low correlation with precipitation amounts in the driving GCM (Fig. S13) and an opposite future change signal (summer precipitation increase instead of a clear summer precipitation decrease in the driving GCM; Fig. S13). Furthermore, the simulated temperature evolution in summer (JJA) and partly also in autumn (SON) is subject to a sudden shift to lower levels around year 2023 (Fig. S14). This feature is not apparent in the driving GCM and cannot be explained on a physical basis. The IPSL-WRF model chain is therefore considered as part of the full model set, i.e. in places where identification of individual models is possible, but is not contained in the reduced model set (see Table 1 of the main manuscript).

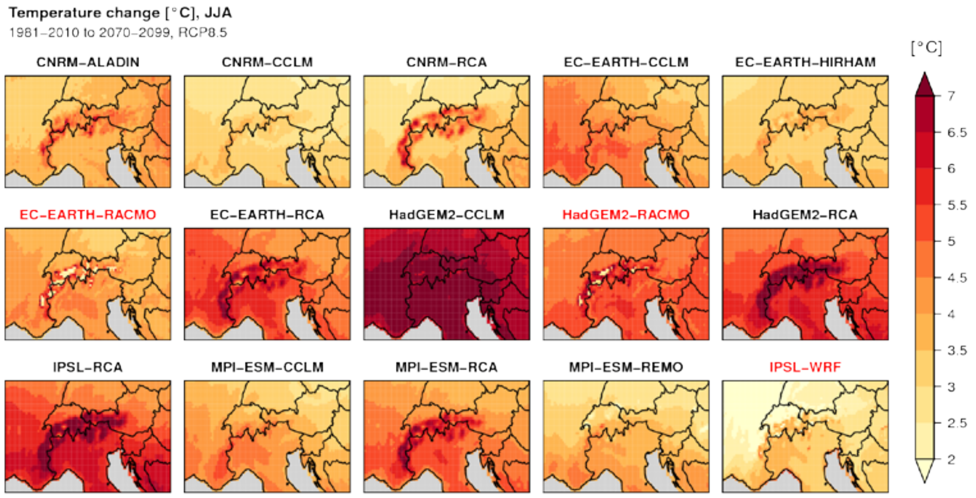

Figure S11 Spatial pattern of summer (JJA) temperature change signals (2070-2099 with respect to 1981-2010) for RCP8.5 in the 15 EUR-11 GCM-RCM model chains that were available in December 2016. Red font denotes models that were either completely or partly removed from our analysis. Note the considerable lower change signal over high-alpine grid cells in EC-EARTH-RACMO and HadGEM2-RACMO.

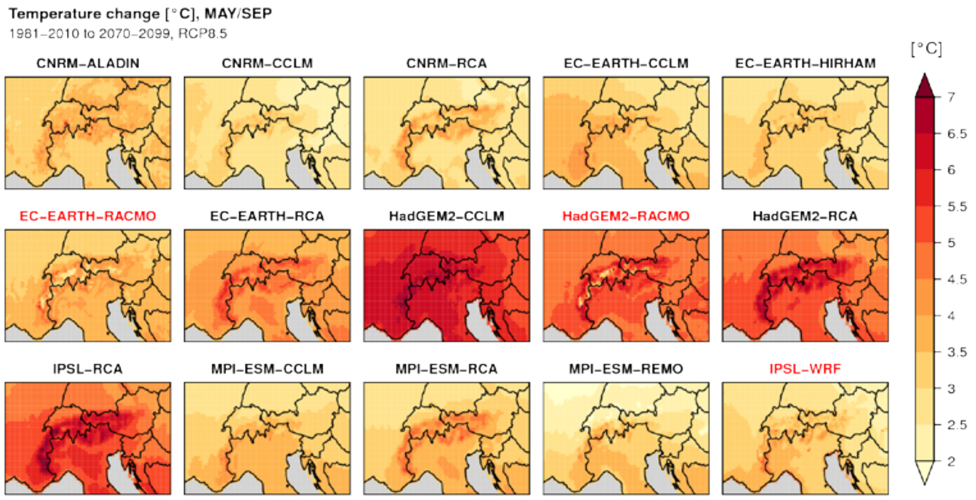

Figure S12 As Fig. S11 but for the mean May/September temperature change signal.

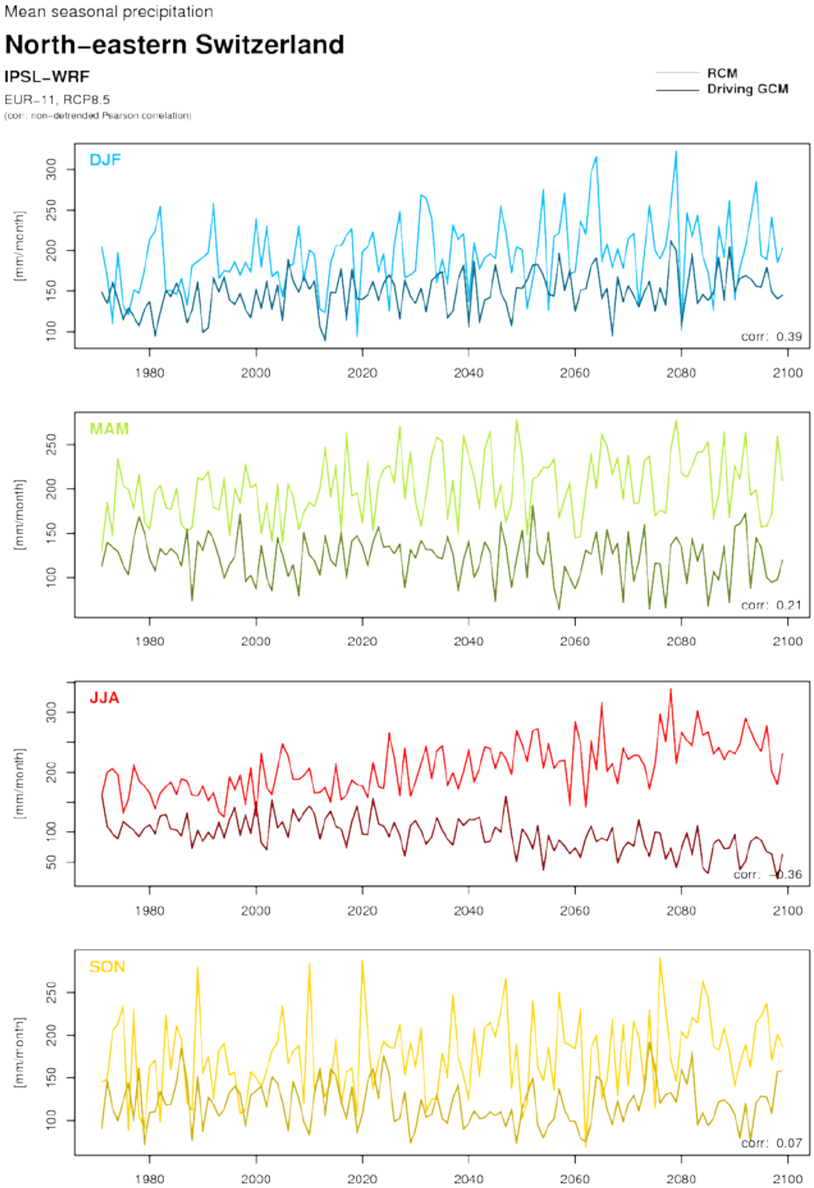

Figure S13 Evolution of seasonal mean precipitation over north-eastern Switzerland in EUR-11 IPSL-WRF for RCP8.5. Dark line: driving GCM (IPSL), bright line: RCM (WRF). The number in the lower right corner of each panel indicates the non-detrended Pearson correlation coefficient of mean seasonal precipitation in the RCM and its driving GCM. Note the negative correlation in summer (JJA) and the opposing summer precipitation trends.

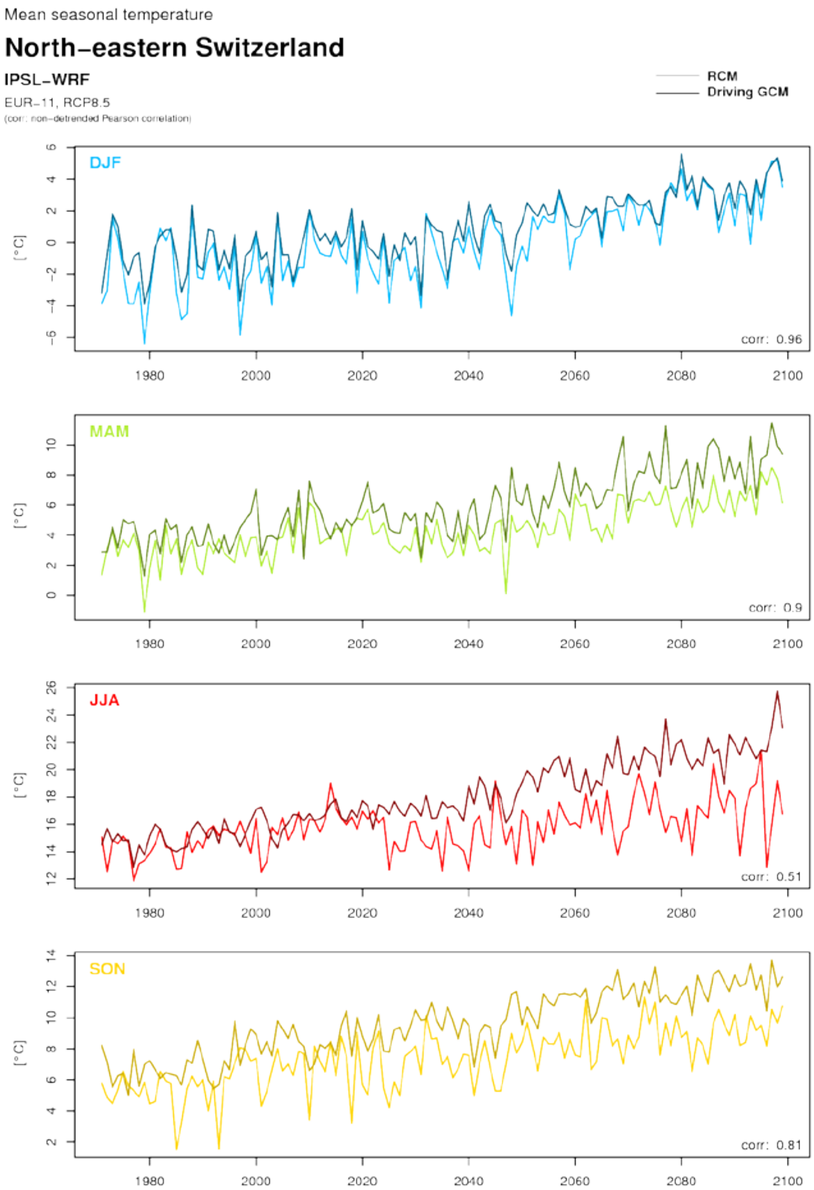

Figure S14 As Fig. S13 but for seasonal mean temperature. Note the low correlations of summer (JJA) temperatures and the apparent shift of summer (JJA) and autumn (SON) temperatures in the RCM around year 2023.

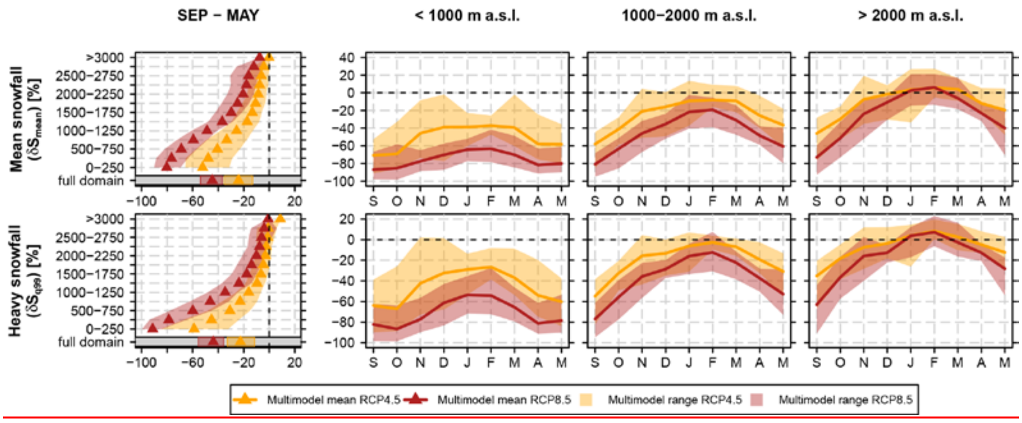

Figure S15 As Fig. 12 of the main manuscript but for the full model set (14 RCM simulations for each emission scenario).